Journal of Volcanology and Geothermal Research 418 (2021) 107325

Contents lists available at ScienceDirect

Journal of Volcanology and Geothermal Research

journal homepage: www.elsevier.com/locate/jvolgeores

Reconstructing eruptions at a data limited volcano: A case study at Gede (West Java)

Eleanor Tennant [a,*], Susanna F. Jenkins [a], Annie Winson [b], Christina Widiwijayanti [a], Hendra Gunawan [c], Nia Haerani [c], Nugraha Kartadinata [c], Wilfridus Banggur [c], Hetty Triastuti [c]

[a] Earth Observatory of Singapore and Asian School of the Environment, Nanyang Technological University, 639798, Singapore
[b] British Geological Survey, Keyworth, Nottingham NG12 5GG, United Kingdom
[c] Center for Volcanology and Geological Hazard Mitigation, Bandung city, West Java 40122, Indonesia

ARTICLE INFO

Article history:
Received 29 December 2020
Received in revised form 16 June 2021
Accepted 18 June 2021
Available online 22 June 2021

Keywords:
Pyroclastic density currents
Titan2D
Tephra fall
Tephra2
Gede volcano
Indonesia

ABSTRACT

Understanding past eruption dynamics at a volcano is crucial for forecasting the range of possible future eruptions and their associated hazards and risk. In this work we use numerical models to recreate the footprints of pyroclastic density currents (PDCs) and tephra fall from three eruptions at Gede volcano, Indonesia, with the aim of gaining further insight into these past eruptions and identifying suitable eruption source parameters for future hazard and risk assessment. Gede has the largest number of people living within 100 km of any volcano worldwide, and has exhibited recent unrest activity, yet little is known about its eruptive history. For PDCs, we used Titan2D to recreate geological deposits dated at 1.2 and c. 1 kyrs BP. An objective and quantitative multi-criteria method was developed to evaluate the fit of 342 model simulations with field observations. In recreating the field deposits we were able to identify the best fitting values to reconstruct these eruptions. We found that the 1.2 kyrs BP geological deposits could be reproduced with Titan2D using either a dome-collapse or a column-collapse as the triggering mechanism, although a relatively low basal friction angle of 6° would suggest that the PDCs were highly mobile. For the 1 kyrs BP PDC, a column-collapse mechanism and a higher basal friction angle were required to fit the geological deposits. In agreement with previous studies, we found that Titan2D simulations were most sensitive to the basal friction angle parameter. We used Tephra2 to recreate historic observations of tephra dispersed to Jakarta and Gunung Patuha during the last known magmatic eruption of Gede in 1948. In the absence of observable field deposits, or detailed information from the published literature, we stochastically sampled eruption source parameters from wide ranges informed by analogous volcanic systems, allowing us to constrain the eruption dynamics capable of dispersing tephra to the most populous city in Indonesia, Jakarta. Our modelling suggests that the deposition of tephra fall in Jakarta during the November 1948 eruption was a very low probability event, with a $< 1\%$ chance of occurrence. Through this work, we show how the reconstruction of past eruptions with numerical models can improve our understanding of past eruption dynamics, when faced with epistemic uncertainty. At Gede volcano, this provides a crucial step towards the reduction of risk to nearby populations through volcanic hazard assessment.

1. Introduction

Approximately 30 million people worldwide live within 10 km of an active, and potentially dangerous, volcano (Brown et al., 2015). Volcanic hazard assessments can support the reduction of risk for these populations by identifying the range of potential future eruption styles and quantifying the spatial distribution and intensity of associated hazards. Due to the complexity of the phenomena, this quantification is often undertaken with the help of numerical hazard models, which are mathematical formulations developed to represent the physical processes that produce volcanic hazards. Model inputs used for forecasting the extent of future hazardous phenomena are often sourced from past eruptions, where possible, using field data and historical accounts (written descriptions of volcanic activity) to characterise the eruption dynamics such as plume height or the mass of pyroclastic material erupted.

However, it is often the case that the information available about past eruptions at a volcano doesn't tell the complete story (Sheldrake and Caricchi, 2017; Beven et al., 2018; Tierz, 2020); and sources of epistemic uncertainty can occur due to: 1) short/incomplete historical records, 2) poor deposit preservation, or 3) difficulty in accessing remote field locations. In light of these knowledge gaps, input parameters required for forecasting the spatial extent of future volcanic hazards have previously been estimated by reconstructing these past eruptions.

* Corresponding author.
E-mail address: etennant@ntu.edu.sg (E. Tennant).

https://doi.org/10.1016/j.jvolgeores.2021.107325

That is, running hazard models with deliberately wide ranges of unknown initial values (e.g. Connor and Connor, 2006), where ranges are informed by the data that *is* available (e.g. Procter et al., 2010; Charbonnier et al., 2013) and are sometimes supplemented through consideration of analogous systems (e.g. Jenkins et al., 2020). The resulting simulation outputs are then compared with field observations of the deposit and from that, input parameters are adjusted, iterating towards the best fitting set of values and constraining the most likely eruption dynamics (e.g. eruption style and size, column height, and flow triggering mechanism, among others). Armed with an improved understanding of past eruptions, volcanic hazard modelling can then be undertaken to forecast the spatial extent of future hazards. This process of fitting model values to field data for the purpose of learning more about the eruption that produced the field deposits can be termed eruption reconstruction. Here we distinguish between using the numerical model to recreate the observations, and, the reconstruction of the eruptive event itself following the subsequent interpretation of the best fitting values.

For volcanic flows, the comparison between the modelled data and the field observations typically considers the flow footprints and maximum runouts, and can be compared in a qualitative (through visual comparison, e.g. Takahashi and Tsujimoto, 2000, Heinrich et al., 2001, Patra et al., 2005, Procter et al., 2010) or quantitative way (e.g. Rupp et al., 2006, Kubanek et al., 2015., Charbonnier et al., 2018). For well-known PDCs additional metrics have been used to evaluate fit, including consideration of velocity, thicknesses, and more localised features such as channel overspill (Charbonnier and Gertisser, 2009; Ogburn and Calder, 2017). For recreation of tephra fallout, the process of fitting model results to field data has been greatly assisted by inversion techniques that automate the search for the best fitting set of parameters (e.g. Connor and Connor, 2006, Bonasia et al., 2010, White et al., 2017); however, for recreating PDCs, due to the computational requirements of simulations a manually iterative process is often adopted (e.g. Procter et al., 2010).

In this work we reconstructed three selected historical eruptions of Gede volcano (west Java, Indonesia), by using numerical models to reproduce PDC deposits, and a historical account of tephra fall associated with those eruptions, we then critically examined the best fitting solutions using these to reconstruct the eruptions. The main objective of this study is to improve our understanding of past eruptions at Gede and the hazards they produced, in addition to identifying best fitting model values that can be used for future hazard modelling at Gede.

1.1. Gede volcano

Gede is an active stratovolcano standing at 2958 m above sea level (a.s.l.), and located 60 km south of Indonesia's capital city Jakarta, a region with one of the highest population densities in the world (Fig. 1). The geological evolution of Gede began in the Pleistocene with the effusive eruption and construction of the main 100 km^3, silica-basalt Gumuruh cone. At the Pleistocene-Holocene boundary, Gede appears to have undergone a repose period of approximately 30,000 years (Belousov et al., 2015), which was followed by a transition in eruption styles from effusive cone building to the dominantly explosive activity of young Gede.

The region around Gede was mapped by the Volcanological Survey of Indonesia (now known as the Center for Volcanology and Geological Hazard Mitigation (CVGHM)) in 1992 (Situmorang and Hadisantono, 1992), this geological information was later used to make the official hazard map for Gede (Hadisantono et al., 2008) which is deterministic and based on field deposits from the past 100 years of eruptive activity. During this time there have been 2 magmatic eruptions, both with a Vulcanian eruption style. More recently, geological studies were undertaken by Belousov et al. (2015) who identified and dated four ancient PDC deposits, providing evidence of explosive eruptions during the Holocene occurring at 10, 4, 1.2, and, 1 kyrs BP. Holocene deposits extend

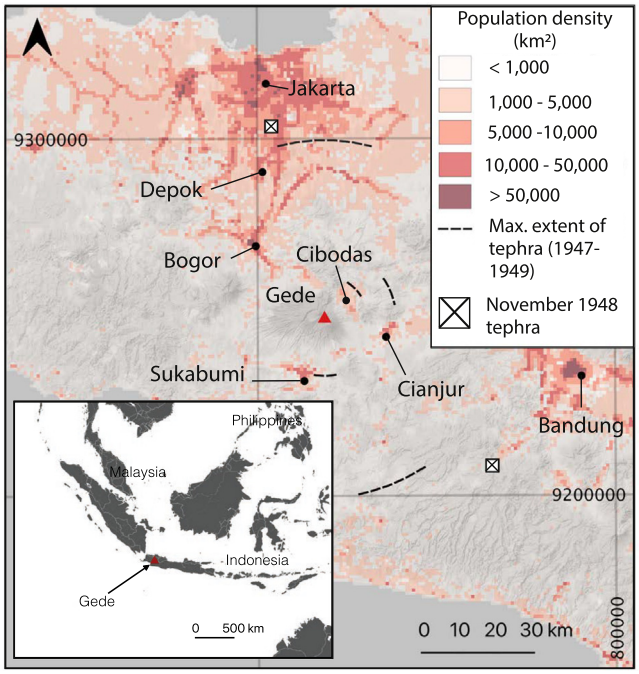

Fig. 1. Population density in the region surrounding Gede volcano. Also marked are the maximum reported tephra extents in several directions for eruptions in the period 1947–1949 (see Section 2.3 for details). Population data source: Landscan 2018 global dataset (Rose et al., 2019). Geodetic system/projection: WGS84/UTM Zone 48S (EPSG: 32748).

up to ~15 km away from the vent in the NE sector (Fig. 2a) and have been attributed to eruptions with Volcanic Explosivity Index (VEI: Newhall and Self, 1982) 2–4 (Belousov et al., 2015). The distribution of these flow deposits is topographically controlled, resulting from the formation, collapse and progradation of eruptive centres over time. Today the Gede crater features breaches towards the N and NE directions. The breaches are separated by a ridge and the remaining piece of crater rim known as 'Sela' ridge. The Gede crater is partially filled by the c.1840 blocky andesitic lava dome, and a lava flow which extends 1.5 km away from the summit towards the NE. The dome is punctuated by several modern craters of small size (Fig. 2b: Ratu, Wadon, Lanang, and Baru). In the NE and SE sectors, debris avalanche deposits evidence previous large-scale collapses, at ca. 920–740 years BP, and > 43,500 years BP respectively (Belousov et al., 2015), the latter of which, underlies the city of Cianjur and travelled at least 35 km. Tephra fall deposits can be found in the proximal area only (Bear-Crozier et al., 2012; Belousov et al., 2015), and are suggested to be characteristic of multiple weak phreatomagmatic/Vulcanian eruptions (VEI 2–3) (Belousov et al., 2015). The first historical account of an eruption at Gede is from 1747. Since then, there have been 23 recorded eruptions, ranging from VEI 1 (n = 3) to VEI 3 (n = 4), with the majority (n = 16) VEI 2. The most recent eruptions, occurred in 1956 and 1957, these were considered of phreatic origin and assigned a default VEI 2 (Global Volcanism Program, 2013). In the process of classifying all known eruptions, the Global Volcanism Program used this default assignation for eruptions that were known to be explosive but no further information was available. This default assignation may also be responsible for the large number of VEI 2 sized eruptions in Gede's record.

Seismometers were installed at Gede by CVGHM in 1985, and later the network was expanded as part of a collaboration between CVGHM and the Earth Observatory of Singapore. Swarms of increased seismicity have been recorded every 1–2 years, (Hidayat et al., 2019) and an analysis of the October 2015 swarm event identified hypocentres between 1.5 km (a.s.l.) and 700 m below sea level with no apparent migration

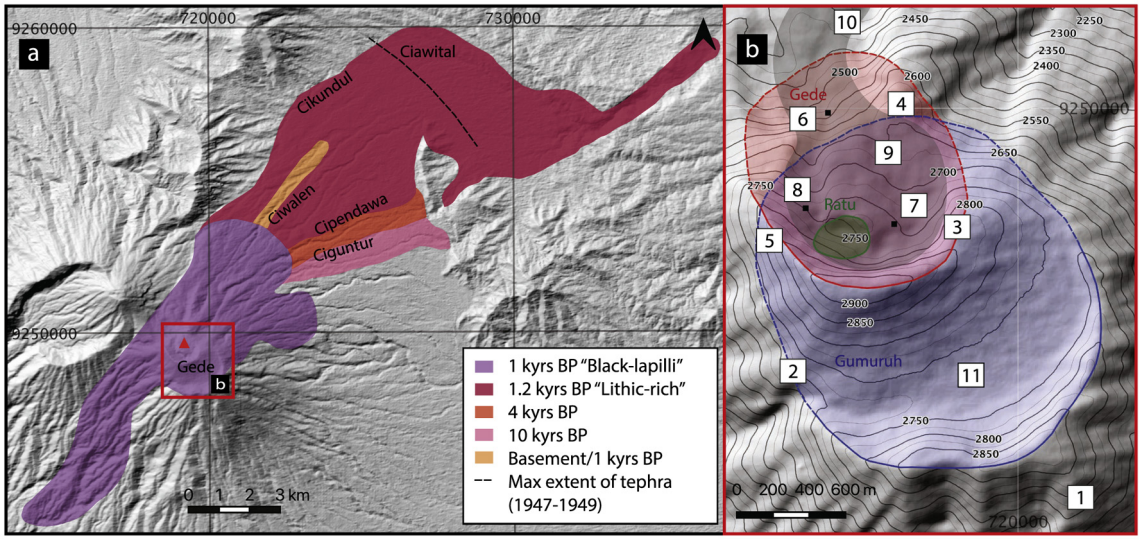

Fig. 2. a) Holocene PDC deposits, adapted from Belousov et al. (2015), inset (part b) shows the present-day summit topography, with the main craters (Kawah in Bahasa Indonesian) in shaded colours. Minor craters are shown with black markers. Key features include 1. The main Pleistocene Gumuruh cone, 2. Kawah Gumuruh (blue), 3. Kawah Gede (red), 4. Sela ridge, 5. Kawah Ratu (green), 6. Kawah Wadon, 7. Kawah Lanang, 8. Kawah Baru, 9. 1840 lava dome (grey shaded area inside Kawah Gede), 10. 1840 lava flow (grey shaded area extending out of the crater), 11. Flat grassy Alun-Alun area. Geodetic system/projection: WGS84/UTM Zone 48S (EPSG: 32748).

(Nugraha et al., 2017). An earlier swarm event (2012) was attributed to movement on the NE-SW orientated fault that runs between Gede and Pangrango (Aryanti et al., 2018). At present, Gede displays persistent fumarolic activity at the summit.

2. Choosing case study eruptions

The recent recorded eruption history (since 1747) is dominated by VEI 2 eruptions, but larger VEI 3–4 eruptions are known to have occurred in the Holocene (Global Volcanism Program, 2013; Belousov et al., 2015). Based on the explosive nature of past eruptions, identified through stratigraphic studies (Belousov et al., 2015) and historical observations (Global Volcanism Program, 2013), there are three main medial to distal hazards from a future eruption at Gede: PDCs, tephra fall and lahars. Here, we focus on reconstructing the triggering, transport and deposition of pyroclastic deposits (flows and falls) produced by three different eruptions in the Holocene: 1.2 kyrs BP, c.1 kyrs BP, and 1948 CE. These eruptions were selected based on a comprehensive search of the literature for records describing eruptions at Gede. This also included visiting and transcribing documents from the CVGHM archives located in Bandung (Appendix A).

With the information collected during our research we decided to reconstruct eruptions that produced PDCs from two of the four PDC-producing eruptions in Gede's past. The 1.2 kyrs BP eruption was selected as a 'worst case scenario' based on recorded events. Mapped PDC deposits from this eruption underlie the densely populated town of Cibodas (Fig. 1) and have a total volume of 0.15 km^3 (Belousov et al., 2015) which the authors split into four units of roughly equal volume. A single unit has a volume of approximately 0.0375 km^3; assuming that one unit was produced by one PDC event, this is the largest of the known historic PDCs at Gede, and is in the upper 96th percentile of PDCs recorded in the Flowdat global dataset (Ogburn, 2012) with a size similar to the 26 December 1997 lateral blast triggered block and ash flow (BAF) at Soufrière Hills volcano, Montserrat (Sparks and Young, 2002). In contrast, the c.1 kyrs BP event, produced a PDC with a considerably shorter runout than the 1.2 kyrs BP PDC. The triggering mechanism proposed by Belousov et al., (2015) for the former is a fountain collapse from a short-lived column, which is in line with the Vulcanian eruption style that is considered typical for Gede (Petroeschevsky, 1952). For the 1.2 kyrs BP PDC Belousov et al. (2015) propose the collapse of a non-buoyant phreatomagmatic plume, erupted through a crater lake (a boiling over type PDC). In recreating these two PDCs we aim to further our understanding of, and identify best fitting model inputs for, the *worst-recorded-case* and a *more typical* PDC-producing eruption scenario at Gede. The case study eruptions are described in detail in Sections 2.1–3, and key properties of the PDC deposits can be found in Table 1.

For the reconstruction of eruptions producing tephra fallout we focused on events that have affected Jakarta, Indonesia's capital city. Today, the transport of tephra to Jakarta has the potential to impact over ten million residents, plus a major international airport and Indonesia's largest seaport. Historical observations (Appendix A) suggest that tephra fall from Gede has reached downtown Jakarta on at least two occasions: in 1832 (VEI = 3) and in 1948 (VEI = 2). The chronology of the 1948 eruption has been described by Petroeschevsky (1952), and the meteorological data for 1948 are provided by the ERA20C European Centre for Medium-Range Weather Forecasting (ECMWF) dataset (Poli et al., 2016). Access to these datasets provided useful constraints on the modelling in absence of other data sources (such as field deposits), enabling reconstruction of the eruption dynamics capable of producing this event. We therefore chose the 1948 eruption to recreate the tephra fallout from.

2.1. 1.2 kyrs BP: Lithic-rich PDC

The largest of the four Holocene deposits described by Belousov et al. (2015), is the 1.2 kyrs BP deposit, which is likely the product of a VEI 3 eruption (Belousov et al., 2015). The deposit is split into four units each

Table 1
Physical characteristics of the Lithic-rich and Black-lapilli PDC deposits from field observations (following data from Belousov et al., 2015).

Property	1.2 kyrs BP: Lithic-rich PDC	c.1 kyrs BP: Black-lapilli PDC
Total volume	0.15 km^3	0.01 km^3
Flow units	4 × 0.0375 km^3	1
Max runout (NE)	14.4 km	4.8 km
Max runout (SW)	–	7 km
Average thickness	3–7 m	1–3 m
PDC footprint	57 km^2	31 km^2

3–7 m thick (locally 20 m thick in the Cikundul valley), with a maximum runout of 14.4 km (Fig. 2a). In this work we assumed units to represent individual PDCs (and hence focus the modelling on recreating one PDC), however given the absence of a depositional gap (Belousov et al., 2015) it is not clear how the boundary between units was defined, and there is the potential that a single unit represents only part of an unsteady PDC. If this is the case, then the volume used in simulations may be too low. Units are geologically similar, consisting of massive, poorly sorted, locally weakly-moderately indurated, ash and lapilli, with a high proportion of non-juvenile clasts. Non-juveniles consist of dense-angular lava clasts, while juveniles are poorly to moderately vesicular scoriaceous basaltic-andesite. The lowest unit contains clasts of well-rounded pumice, suggesting the presence of a buoyant column prior to PDC triggering. In this work we recreate a single PDC (unit) of the 1.2 kyrs BP deposit with a volume of 0.0375 km^3. Throughout the text we use 'Lithic-rich PDC' to refer to one unit of the 1.2 kyrs BP deposit.

2.2. c.1 kyrs BP: Black-lapilli PDC

The youngest of the Holocene deposits, the 'Black-lapilli' PDC (Belousov et al., 2015) is small in comparison to the other Holocene PDCs, with a maximum thickness of 1–3 m and a total volume of 0.01 km^3. Maximum runout is 4.8 km towards the NE and 7 km towards the SW. The deposit is massive, moderately sorted and is depleted in fines. The majority of clasts are juvenile, moderately vesicular and of basaltic-andesitic composition. This PDC postdates the north-eastern collapse of the Gede crater wall, and the draining of the crater lake, and is interpreted to have been the product of a collapsing fountain from a small, dry, explosive eruption of VEI 2–3 (Belousov et al., 2015).

2.3. 15–23 November 1948 eruption

The chronology of the most recent magmatic eruption at Gede is described in the work of Petroeschevsky (1952) (Appendix B), therefore this is the primary source of information used to reconstruct this event. According to Petroeschevsky (1952), the eruption started on 15 November following 10 months of quiescence, with a total of five discrete explosions over the following 8 days that generated eruptive columns up to 5 km above the vent. Field deposits from these explosions are limited to the proximal area, however Petroeschevsky (1952) describes tephra falls at two distal locations: i) near Gunung Patuha, 62 km SE of Gede, following the 20 November explosion, and ii) in Jakarta, 50 km N of Gede, after the final explosion on 23 November. Petroeschevsky (1952) also details the extent of tephra fall throughout the observation period spanning 1947–1949 as follows: "In southern direction the ash reached 16 kilometres in S.S.E direction 50 kilometres, in E.N.E direction 20 kilometres, in N.E direction 12 kilometres and in northern direction 50 kilometres"; during this time there were two eruptions (as defined according to the Smithsonian Global Volcanism Program). These approximate distances are marked on Fig. 1.

3. Reconstructing PDC producing eruptions using Titan2D

PDCs are typically density stratified, and consist of a particle concentrated basal layer, and a dilute upper surge layer (Branney and Kokelaar, 2002). In the long-term stratigraphic record, fully dilute PDCs and surges are rarely preserved (Kilgour et al., 2019), and deposits are often left with only the dense basal portion of the flows preserved. We used the numerical model Titan2D (Patra et al., 2005) to recreate the preserved dense basal portion of the Lithic-rich and Black-lapilli PDCs. However note that upon deposition the surge portion of these flows is likely to have spread over a wider extent. Titan2D solves depth-averaged shallow water equations for conservation of mass and momentum, applying a coulomb-type frictional resistance model characterised by user input values for basal and internal friction angles. The model was developed to simulate granular flows over Digital Elevation Models (DEMs) of natural terrain (Patra et al., 2005) and has been successfully applied to the simulation of PDCs at multiple volcanoes worldwide including: Merapi volcano, Indonesia (Charbonnier and Gertisser, 2009); Tacaná volcanic complex, Mexico-Guatemala (Vázquez et al., 2019); Mount Taranaki, New Zealand (Procter et al., 2010); Soufrière Hills Volcano, Montserrat (Widiwijayanti et al., 2007; Ogburn and Calder, 2017); Colima volcano, Mexico (Rupp et al., 2006); Cerro Machin volcano, Colombia (Murcia et al., 2010); El Misti volcano, Peru (Constantinescu et al., 2011; Sandri et al., 2014).

3.1. DEM

For our study, we used the Indonesian national DEM known as DEMNAS (Geospatial Information Agency, 2018), which combines IFSAR, TERRASAR-X, and ALOS earth observation data with an acquisition date interval between 2010 and 2015. We reformatted the DEM for use with Titan2D (including up-sampling the resolution from 8.3 m to 10 m). Fluvial processes such as channel incision, erosion and deposition, are likely to have impacted the topography in the many years following PDC emplacement, and obtaining accurate pre-PDC topography is one of the most challenging aspects of numerically recreating PDCs. In some studies, this has been overcome through adjustment of the DEM to represent pre-PDC conditions (e.g. Charbonnier et al., 2013; Vázquez et al., 2019); unfortunately, due to the age of our deposits, and the absence of well distributed thickness measurements, we do not have a model of the pre-PDC topography. Nevertheless, given the NE distribution of PDCs and the present day N-NE orientated crater opening we can assume that the crater topography at the time of emplacement was similar to that of today. Therefore, adjustment was not considered necessary for our study and we decided to run the simulations using the DEMNAS DEM with no modification, in line with previous studies faced with the same challenge (Sheridan et al., 2005; Rupp et al., 2006; Procter et al., 2010). However, we do note that the input DEM is likely to represent one of the key areas of uncertainty in this study.

3.2. Stopping criteria

In Titan2D, the simulated PDC never comes to a complete standstill (Charbonnier and Gertisser, 2012), instead the user must decide an appropriate duration at which time the velocity is low enough that the flow can be considered stationary. For pile collapse simulations, the appropriate flow duration is correlated with the basal friction angle (Tierz et al., 2018). We identified this duration graphically by plotting the average velocity output by the model (across the entire PDC at each time-step) vs time for a number of simulations run at each basal friction angle included in the study. In a given simulation, the average flow velocity first increases to a maximum before decreasing down towards (but not reaching) zero. We picked the breakpoint of these curves, where the average flow velocity approaches zero, and set the simulation duration in accordance with the breakpoint for each basal friction angle (Appendix C). This approach has also been used by Ogburn and Calder (2017) to identify appropriate simulation durations. In all cases, the average velocities picked using this method reach less than 4 m/s, a value at which the flow front propagation is minor and can be considered as stationary (Murcia et al., 2010). For fluxes, the duration is dependent on both the basal friction angle and the flux rate, and so for these cases we considered each simulation separately.

3.3. Material model

Historically, the friction angles used in Titan2D have been acquired either through tabletop laboratory experiments (Iverson et al., 1998; Bursik et al., 2005), or (for basal friction angles) through calculation of the Heim coefficient (the ratio between the drop height and runout length of a flow: Heim, 1932). The basal friction angle is a key control

on flow mobility, with lower values resulting in increased flow runouts (Sheridan et al., 2005; Dalbey, 2009; and Charbonnier and Gertisser, 2012). We used the Heim coefficient, converted into degrees, as our initial parameterisation for the basal friction angle leading to 8° and 13° for the Lithic-rich and Black-lapilli PDCs, respectively. For both PDCs the drop height was calculated by subtracting the altitude of the toe from the vent altitude. Given that the column height is unknown for potential column-collapse type flows, it was not considered appropriate to account for this in the calculation. However, it should be noted that if a column of 2.5 km (collapse height 250 m) was included for the Black-lapilli PDC calculation, this would increase the initial basal friction angle from 13° to 15°. Nevertheless, it has been suggested that the Heim coefficient is highly sensitive to localised changes in topography (Legros, 2002). Given these uncertainties, the values of basal friction angles determined using the Heim coefficient should be considered as initial estimates only. Past work has suggested relative insensitivity to the internal friction angle; assuming that values fall within a reasonable range of 25–45° (Sheridan et al., 2005; Dalbey, 2009), this has led many studies to use a fixed value of 30° (Macías et al., 2008; Charbonnier and Gertisser, 2009; Sulpizio et al., 2010; Vázquez et al., 2019). We examined the sensitivity to this parameter for the Lithic-rich PDC using a pile source type and simulating across the 25–45° range.

3.4. Source characterisation

In Titan2D, different types of PDCs can be modelled, depending on their triggering mechanism, using different source terms, that reflect the mobility variations among the flows (Rutarindwa et al., 2019). As an example, the 'collapsing-pile' source term, is used to reproduce block-and-ash flows formed during a dome-collapse event (e.g. Procter et al., 2010; Rupp et al., 2006), while a 'flux' source term can be used to model the collapse of a non-buoyant pyroclastic column, allowing for material to actively extrude from the ground (e.g. Ogburn and Calder, 2017). PDCs resulting from a collapsing vertical column have also been simulated with Titan2D using a tall narrow pile source with initial velocity > 0 m/s (Murcia et al., 2010, Constantinescu et al., 2011, Sandri et al., 2014, Paone and Yun, 2016, Rutarindwa et al., 2019. In this work we tested several different source representations (geometries and triggering mechanisms) for each of the case-study PDCs, splitting different source representations into simulation subsets (SS) (numbered SS1-6), all of which are summarised in Fig. 3, and described in more detail in the following sections. The full list of simulations and input parameters can be found in the supplementary material.

3.4.1. 1.2 kyrs BP: Lithic-rich PDC

For the Lithic-rich deposit, Belousov et al. (2015) suggested a non-buoyant explosive phreatomagmatic eruption as the triggering mechanism. However, given the low depositional temperature, and relatively low proportion of juvenile material reported (Belousov et al., 2015), we consider the potential for an alternative triggering mechanism, using the different source options in Titan2D to also test the viability of a dome collapse hypothesis. We therefore modelled this PDC using both 'flux' (SS1) and 'collapsing pile' (SS2-3) source terms (Fig. 3).

For well characterised PDCs, extrusion flux rates can be estimated from the total volume of the field deposit and observations of the

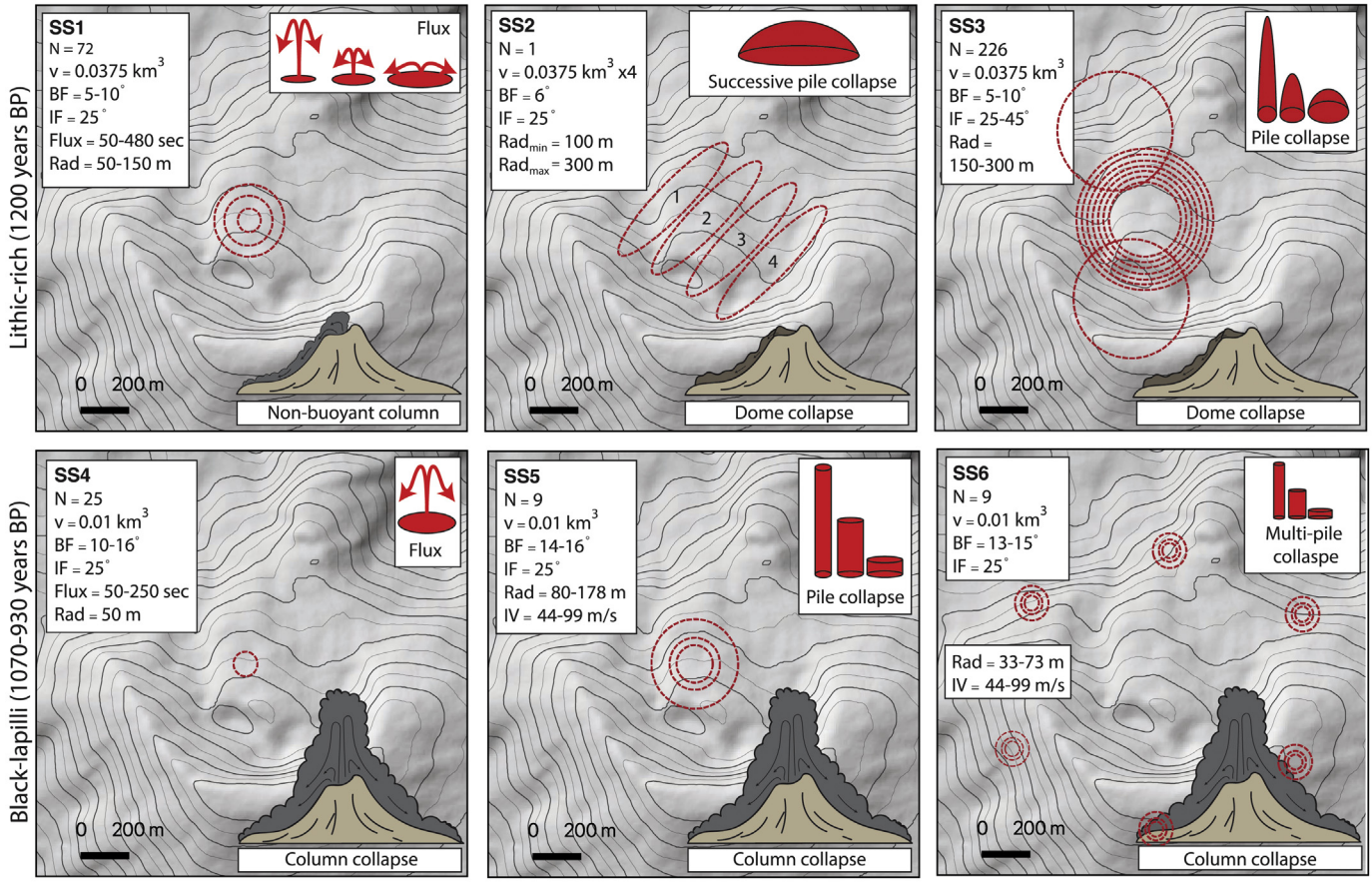

Fig. 3. Titan2D modelling strategy (source representation) for each subset of simulations (SS1-6), and the number of simulations run (N). Top row: simulations run for the 1.2 kyrs BP deposit, bottom row: simulations run for the 1 kyrs BP deposit. Proposed PDC generation mechanisms are pictured bottom right of each panel. Titan2D source types are top right. Red dotted lines represent the location and size of the source term. Input parameters shown are: v - simulated volume, BF- basal friction angle, IF - internal friction angle, Flux - flux duration, Rad - radius of source, IV - initial velocity. Sources are plotted on the Indonesian National DEM (DEMNAS).

eruption duration. In absence of information for collapse durations at Gede we set a relatively wide duration range of 50–480 s, informed by Vulcanian fountain-collapse PDCs at Soufriére Hills volcano (Druitt et al., 2002). PDCs produced by the 1997 eruption of Soufriére Hills are some of the best-observed and studied in the world and provide some of the only collapse durations that are available in the literature. Deposit volume and extrusion durations were used to calculate discharge rates (m^3/s) and extrusion flux rates (m/s) using crater radii informed by the dimensions of the three post-1840 explosive centres (75–150 m diameter). In SS3 (Fig. 3), we tested the dome collapse mechanism hypothesis using a single pile with radial dimensions between 150 and 300 m. Indeed, an initial radius of 150 m is in accordance with the dimensions of the present day Ratu crater, while the remnant andesitic dome (c. 1840, (Belousov et al., 2015)) within the Gede crater has a radius of approximately 400 m (hence a maximum of 300 m was used to ensure that the collapsing pile was constrained inside the Gede crater). The pile height range required to keep the volume consistent across all simulations (0.0375 km^3) is 265-1061 m. Currently the actual location from which the Lithic-rich PDC originated, is unknown, therefore in SS3 we tested three potential start locations, Kawah (crater in Bahasa Indonesian) Ratu, Kawah Gede, and Kawah Wadon (Fig. 2b). Whilst the formation of Ratu and Wadon craters post-dates the PDC (Belousov et al., 2015), they provide reasonable start locations that are alternative to the centre of the Gede crater. Testing these start locations also allows for an assessment of the impact of crater topography on PDC distribution at Gede. In SS2, we simulated a succession of collapse events (each 0.0375 km^3) within the Gede crater (Fig. 3).

3.4.2. c.1 kyrs BP: Black lapilli PDC

The triggering mechanism for this PDC, as suggested by Belousov et al. (2015), is a fountain collapse from a short-lived column, resulting from a 'moderately explosive VEI 2-3 sized eruption'. Three different approaches were used to model this PDC. In SS4 (Fig. 3), fluxes were calculated from the durations reported by Druitt et al. (2002) as described above, using a narrow pile radius of 50 m. In SS5 and SS6 the PDC was modelled as a tall and narrow collapsing pile, with an initial velocity (v) calculated using the following relationship between potential and kinetic energy:

$$v = \sqrt{2gh} \tag{1}$$

where g is the gravitational acceleration (9.81 m/s^2) and h, the collapse height (in meters). We set column heights of 1, 2.5, 5 km above the vent, corresponding to a VEI 2 or a low VEI 3 sized Vulcanian style eruption, it is worth noting that the lower column heights are a sensible choice given the deposit distribution in the NE and SW sectors only. To maintain a consistent volume of 0.01 km^3, pile radii were 178, 113, and 80 m for 1, 2.5, 5 km heights respectively. Assuming that collapse occurs at approximately 10% of the total column height (Wilson et al., 1978), initial velocities were calculated using Eq. (1) as 44, 70, 99 m/s. In SS6 we used a 'multi-pile' source term, comprising six smaller piles with equal volumes positioned radially around the Gede crater (after Constantinescu et al., 2011, Tierz et al., 2018). Using multiple smaller piles, we aim to represent the impact locations of a collapsing eruptive column. In SS6 the collapse heights and initial velocities were the same as those used in SS5, but with the radii adjusted to account for the partition of the total volume across the six piles.

3.5. Assessing goodness of fit

To measure goodness of fit between simulated PDCs and field deposits, many validation studies rely on the visual inspection of flow footprints along with metrics such as runout, and deposit thickness (e.g. Patra et al., 2005; Charbonnier and Gertisser, 2009; Ogburn and Calder, 2017). However, to date there is no strict procedure for the combination of quantitative metrics used for fitting. In this work, we deliberately developed a more objective and repeatable method when evaluating the goodness of fit between model results and reality. Two quantitative metrics ($\theta_{1,2}$) were calculated and combined with equal weighting to produce an overall measure of similarity (S), a parameter with values that lie between 0 and 1. One is a perfect fit across both metrics ($\theta_{1,2}$) therefore the numerical simulations with the highest value of S were considered the best fit, and the corresponding model input values and source representation (i.e. mechanism, frictional values, and geometries) were used to make inferences about the eruptions that produced the deposits. $\theta_{1,2}$ are defined as follows:

θ_1 is the difference between the maximum deposit runout (RO_{Field}) and the simulated PDC runout (RO_{Model}), (with runouts measured as the horizontal straight-line distance),

$$\theta_1 = \frac{RO_{Model} - RO_{Field}}{RO_{Field}}. \tag{2}$$

Values of θ_1 range from −1 to 1, where positive values indicate that the value obtained with the model is greater than the field data value, and vice versa, therefore a value of 0 means that the modelled value is equal to the field data. For integration into S, we do not differentiate between positive and negative values of θ_1, and negative integers are converted into positive integers which allows S to lie between 0 and 1. We then subtract values from 1, enabling a value that lies closer to 1 to describe a better fit.

θ_2 is a parameter related to the assessment of the PDC footprint, through calculation of the Jaccard similarity coefficient; which measures the statistical similarity between two datasets. Here θ_2 is used to compare simulated and deposit-derived footprints across the simulation grid. In Titan2D, to avoid unrealistically thin deposit thicknesses in computational cells on the external margin of the simulated flow, the user needs to specify the minimum thickness required to define the flow outline. For this we use a value of 10 cm, in line with the abrupt terminations of pumice flow deposits produced during the 1995 eruption at Soufrière Hills Volcano, Montserrat, which lie between 0 and 1 m (Calder et al., 1999). θ_2 is defined as follows:

$$\theta_2 = \frac{TP}{TP + FN + FP}, \tag{3}$$

where TP is the number of cells that are true positives (i.e. areas inundated by both the simulated PDC and the field deposit), FN are false negatives (cells inundated by the field deposit, but not the simulation), and false positives (FP) (cells inundated by the simulated PDC, but not the field deposit). A value of 1 represents the perfect fit between field observations and the simulated deposit. This approach has been applied to evaluate lahar models at Panabaj, Guatemala (Charbonnier et al., 2018).

3.6. Sensitivity analysis

We simulated PDCs across a broad range of input parameter space to find those that best fit the field deposits. Given the number of simulations that we ran, this provided a large enough simulation set to conduct an in-depth sensitivity analysis. This analysis allowed us to recognise the influence of each input parameter in varying the model output, and therefore understand which parameters are more important to constrain. A simple test of sensitivity looks at how much percentage change in the input parameter affects the percentage change in the output (Sheridan et al., 2005), by varying one parameter at a time (OAT testing). Using this approach, we examined the sensitivity of our output parameters: the maximum runout, and the PDC footprint (the raw value as opposed to JC), to all of the input parameters that were varied to fit the deposits. To test the sensitivity of outputs to a particular input parameter all other parameters should remain fixed. Therefore, given the differences in the source types between the simulation subsets; we examined the sensitivity to the input parameters separately in each simulation subset (i.e. we cannot compare the effect of varying the basal

friction angle in a flux type source with a pile type source because all other parameters should remain fixed). Table 2 shows the input parameters that were the subject of the sensitivity testing, and the simulation subsets that they were tested in.

We used a moving window to assess the sensitivity of the parameters and calculated the percentage change in outputs between consecutive incremental increases in the inputs, instead of choosing one simulation and varying the input parameters away from this single simulation (the convention with OAT testing). This is valuable as the relationship between the inputs and measured outputs is not always linear for simulations run over natural terrain. Indeed, if the initial volume is maintained, then increasing the pile radius from X to Y will reduce the pile height which may then cause a reduction in momentum and runout. Increasing the radius further however, may cause a more dramatic reduction in runout if material is spread between channels. Our approach is illustrated as follows (and in Fig. 4) using sensitivity testing of the basal friction angle within SS1 as an example: SS1 consisted of 72 runs with a range of basal friction angles simulated in 1° increment increases between 5° and 10° for 3 different pile radii and 4 different flux durations. For each basal friction angle increment (5–6°, 6–7°, 7–8° and so on) simulation pairs consist of those in which all other input parameters are identical besides the basal friction angle (these are represented by cells of the same colour in each pair over overlapping matrices in Fig. 4). Percentage change in the outputs was calculated for each simulation pair. This gave a total of 3 radii × 4 flux durations x 5 basal friction angle increments (or 60 data points) each for the impact of basal friction angle on runout, and PDC footprint. Similar matrixes can be imagined for the other input parameters tested and simulation subsets. Using this moving window method, we built a distribution for the sensitivity of each input parameter on the two measured outputs as opposed to a single value, this allows for the identification of variations between different input parameter increments.

4. Reconstructing the 1948 eruption

Tephra fall deposits from the 1948 eruption are limited to the summit area of the volcano, however we know from the historic account of Petroeschevsky (1952) that trace amounts of tephra fall were reported close to Gunung Patuha and Jakarta, following the explosions of 20 and 23 November respectively (Fig. 1). Reconstruction of the 1948 eruption at Gede focusses on identifying the dynamics of the eruption capable of causing tephra fall in these locations. To recreate the reported tephra fall, simulations were run using the tephra dispersion model Tephra2 (Bonadonna et al., 2005) within the MATLAB probabilistic wrapper TephraProb (Biass et al., 2016a). Tephra2 is based on a simplified two-dimensional solution to the advection-diffusion-sedimentation equation and has been widely applied to both the forecasting of future tephra fall (Volentik et al., 2009; Biass et al., 2016b; Biass et al., 2017; Tsuji et al., 2017) and the reconstruction of past events (Johnston et al., 2012; Jenkins et al., 2020; Williams et al., 2020). Tephra2 outputs tephra accumulation across the simulation grid in kg/m^2, however the historic report of Petroeschevsky (1952) doesn't give any quantitative indication of mass accumulation at the two locations, therefore, to compare between our simulated tephra fall and the report, we assumed the tephra fall accumulation to be minor, yet sufficient enough to be noticeable. Magill et al. (2013) found that a thickness of 0.5 mm (approximately 0.5 kg/m^2) was enough to cover road markings, and so we considered a lower threshold of 0.1 kg/m^2 to represent trace amounts of tephra fall sufficient enough to be noticeable to residents at the reported locations of Gunung Patuha and Jakarta. Wind conditions (speed and direction with height) for the dates of the eruption were downloaded from the ECMWF atmospheric reanalysis dataset ERA20C (Poli et al., 2016). The dataset provides 3 hourly values at 37 different pressure levels with a horizontal resolution of approximately 125 km.

The two explosions of 20 and 23 November were simulated separately with eruption source parameters (ESPs) (plume height, erupted mass, total grain size distribution (TGSD), and amount of aggregation) and meteorological conditions either fixed, or stochastically sampled from ranges of these variables. Ranges were used to reflect the epistemic uncertainty in source parameters. Four scenarios were run for each explosion, each scenario consisted of 10,000 simulations, and each simulation had a different combination of the unknown parameters. Consecutive scenarios were progressively less constrained by the 1948 event until the threshold amount of tephra accumulation was exceeded at the historically observed locations. In this way we aimed to simulate a wide range of all potential ESP and meteorology combinations to find the combinations that were able to produce tephra fall at the two reported locations. All ESPs are given in Table 3.

The modelling conditions were set as follows:

Scenario 1: Wind conditions were fixed according to the closest wind profile to the time of the explosions (i.e. the 20, 23 November), and column heights were set at 2 and 2.5 km above the vent as reported by Petroeschevsky (1952).

Scenario 2: Wind conditions were sampled from a 10 year dataset centred on 1948 (1944–1953), with column height values as reported by Petroeschevsky (1952).

Scenario 3: Wind conditions were fixed according to the closest wind profile to the time of the explosions (i.e. the 20, 23 November), and column height values were sampled from a uniform distribution between 1 and 15 km above the vent. The column height range was chosen as the minimum of a VEI 2 sized eruption and extended to the maximum of a VEI 3 sized eruption.

Scenario 4: Wind conditions were sampled from the 10 year dataset and column height values were sampled from a uniform distribution between 1 and 15 km above the vent.

Table 2
Input parameters varied in each simulation subset for the sensitivity analysis.

Input parameter	Simulation Subset	Values tested
Start location	SS3	Gede crater, Wadon crater, Ratu crater
Basal friction angle	SS1	5, 6, 7, 8, 9, 10°
	SS3	5, 6, 7, 8, 9, 10°
	SS4	10, 12, 14, 15, 16°
	SS5	14, 15, 16°
	SS6	13, 14, 15°
Internal friction angle	SS3	25, 30, 35, 40, 45°
Pile radius	SS3	150, 175, 200, 225, 250, 275, 300 m
Flux duration	SS1	50, 100, 240, 480 s
	SS4	50, 100, 150, 200, 250 s
Initial velocity	SS5	44, 70, 99 m/s
	SS6	44, 70, 99 m/s

5. Results

5.1. Reconstructing PDC producing eruptions

Titan2D could be applied to accurately reproduce travel paths, and coverage areas for both of the historical PDCs at Gede. The Lithic-rich PDC deposit could be reproduced using either a 'flux' (SS1) or a 'collapsing pile' (SS3) source term. For the 'successive collapsing pile' source term (SS2), in order to fit the large total deposit volume (0.15 km^3) within the Gede crater, the maximum height of the initial individual pile sources was ~800 m. Collapse from this height resulted in inundation of the E, SE, and SW flanks in addition to the NE direction. Goodness of fit matrices are presented for SS1 and SS3 (Fig. 5); red text depicts the best fitting simulation in each. For θ_1 (runout), white and pale-yellow cells represent simulations that are a better fit to the field deposit, with those towards the red and blue ends of the scale representing simulations in which the model overestimated or underestimated the field observation value, respectively. For θ_2 (PDC footprint), yellow cells suggest a perfect fit between the simulated PDC and the field deposit. The

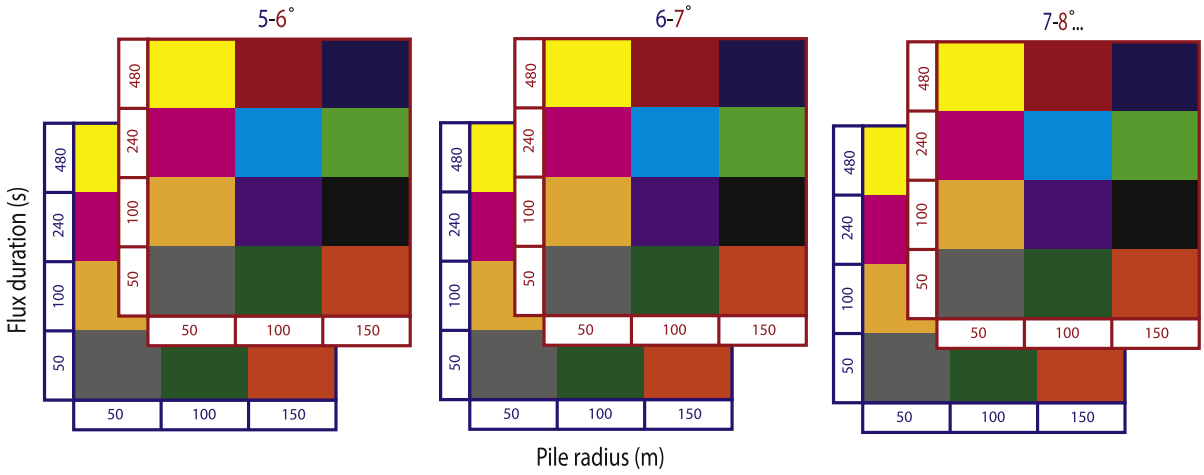

Fig. 4. A graphical representation of the methodology used to investigate the sensitivity of Titan2D measured output parameters (runout and PDC footprint) to the model inputs. The example given is for the basal friction angle in simulation subset 1. For overlapping matrices percentage change is calculated between grid cells with the same flux duration and pile radius (corresponding colours), enabling a percentage change distribution to be built as opposed to a single value.

Table 3
Ranges of input parameters stochastically sampled by Tephra2 simulations, and their rationale. In brackets is the extended plume height range used for Scenarios 3–4.

Input parameters	Values	Rationale & reference
Vent height	3008 m	Global Volcanism Program (2013)
Plume height (km above vent)	2, 2.5 km, (1–15 km)	Reported heights from Petroeschevsky (1952).
Erupted mass	Explosions are considered instantaneous. The mass is calculated from the plume height using the thermal equation of Bonadonna et al. (2002)	
Particle size bounds	−7-7 ϕ	TGSD for the 1979 Soufrière St Vincent (SSV) eruption (Brazier et al., 1982).
Median grain size	1–3 ϕ	Gede has an active hydrothermal system, and recent phreatic eruptions suggest that water might have played a role in the November 1948 eruption. We therefore consider the phreato-vulcanian eruption of SSV as a good analogue for TGSD.
Standard deviation	1–3 ϕ	
Aggregation	30–70% particles <63 μm	Conservative estimate for proportion of particles <63 μm falling as aggregates (Sparks et al., 1997)
Eddy constant	0.04	Eddy diffusion value for Earth for small particles (Suzuki, 1983)
Diffusion coefficient	4900	Best fitting inversion values for Fuego volcano (Guatemala) 1974 (Biass et al., 2016b), an eruption characterised by pulsatory activity cycling between Vulcanian and Sub-plinian behaviour.
Fall time threshold	5000	
Lithic density	2300 kg/m^3	Proximal tephra sampled at Gede, (Bear-Crozier et al., 2012)
Pumice density	935 kg/m^3	
Column steps	100	Reflects a maximum distance between vertical tephra point sources of 150 m.
Particle steps	20	TGSD is split into bins of width 0.7 ϕ in line with the work of Bonadonna et al. (2002)
Plume model	Beta distribution $\alpha = 1, \beta = 1$	A uniform mass distribution provided the best fit for Vulcanian explosions at Montserrat 1997 (Bonadonna et al., 2002)

single best fitting simulations from the two subsets have the same values for θ_1 (0.03) and very similar for θ_2 (0.63 and 0.62). Fig. 5 shows that for both source types, the greatest similarity (S) values were found with a basal friction angle of 6°.

For a flux source (SS1: Fig. 5), with a basal friction angle of 6°, short duration fluxes (50 s) best reproduced the deposit footprint, while the flux duration had little effect on the runout. Instead, we found that the duration of the flux plays a role in the distribution of the deposited material, and fluxes with a higher rate for a shorter duration resulted in a greater amount of material in the Cikundul channel, while for longer duration fluxes the material was less channel confined. The least similarity was found for simulations using basal friction angles of 9–10° with longer duration fluxes, showing the combined importance of basal friction angle and flux duration in controlling the features of the resulting deposits. For the pile-collapse source type simulations (SS3: Fig. 5), the greatest similarity values were found, with a relatively high pile radius (225–300 m). The footprints of best fitting simulations from the two subsets are shown in Fig. 6. While both source types were able to reproduce the PDC footprints well, the best fitting simulation from SS3 resulted in greater deposition in the Cikundul channel, with thicknesses of up to 50 m locally, greatly exceeding the 20 m maximum thickness reported by Belousov et al. (2015). Simulation thicknesses of 50 m occurred at two locations along the channel: 1) Approximately 1 km from the initiation point, where the PDC meets the Cikundul channel and bends towards the NE, and 2) at the Cibereum waterfall ~3.5 km from the source where the channel drops by 60 m. In SS1, the deposit thickness observed in the Cikundul channel was generally lower than is seen in the field.

For simulations run as part of SS3 we tested several different source starting locations, finding that when the Wadon crater was used as the start location, a higher proportion of material entered the Cikundul channel meaning that less was available to the Cipendawa and Ciguntur channels further towards the east. When the Ratu crater was used as the start location, due to its proximity to the steep southerly Gede crater wall (200 m high) material over-spilled the Gede crater and inundated the SW flank of the volcano. Given the observed NE distribution of this PDC, these findings support the likelihood of a central or northerly starting point within the Gede crater for the generation of the Lithic-rich PDC. Well distributed thickness measurements collected in the field would provide better constraints on this.

We found the multi-pile source (SS6) the best source type for recreating the Black-lapilli PDC at Gede, given that this was the only source model able to reproduce flow deposits on the SW flank in addition to the NE. Where the simulations using a flux source representation (SS4) underestimated the PDC footprints, the single pile source in the centre of Gede crater (SS5) produced run-outs comparable with the field deposit but limited to the NE sector. The best fitting results were achieved using an initial velocity of 99 m/s and a basal friction angle of 14° (Fig. 7). The best fitting parameter spaces for simulation subsets SS4-6 are shown in the matrices of Appendix D.

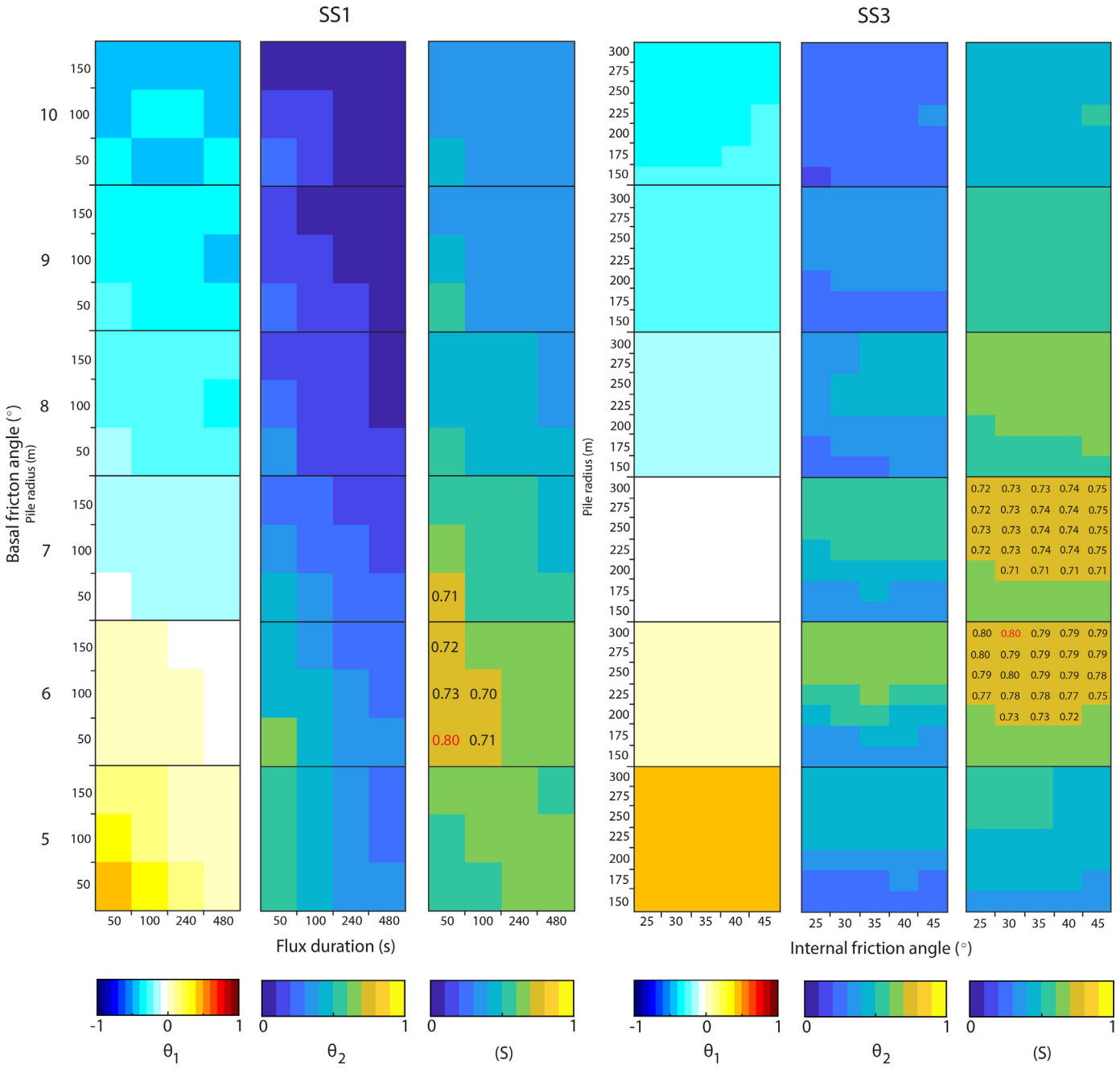

Fig. 5. Matrices showing goodness of fit between simulations and the 1.2 kyrs BP field deposit for simulations run using a flux type source mechanism (SS1) and a pile type source mechanism (SS3). Displayed are parameter spaces for fitting to the maximum flow runout (θ_1), and assessment of the inundation area through calculation of the Jaccard similarity coefficient (θ_2). For maximum runout, simulations that were a better fit to the field deposit are in white/pale yellow, simulations that over-predicted the measure are towards the red end of the colour scale, and simulations that under predicted the measure are towards the blue end. For θ_2, a value of 1 represents the perfect fit between the field deposit and simulations. Overall weighted goodness of fit is defined by S, where 1 is the perfect fit across both metrics. The highest values of S for each simulation subset are shown in red text, with values given for all those with $S > 0.7$.

5.2. Sensitivity analysis

The results of our sensitivity analysis are presented in Fig. 8. The calculated percentage change in output was normalised to a 1% change in each input increment to allow like-for-like comparison across parameters and values (i.e. from a basal friction angle of 5–6° is a 0.2% increase, while from 6 to 7° is a 0.167% increase, both inputs and outputs are normalised to 1%). The mean values for each distribution (μ) are also given. Where distributions are more spread about the mean this suggests that there is some variation in the effect of the input parameter over the outputs, at different input parameter increments.

To compare between input parameters, and understand the most influential of those tested, the population of means was split into three intervals by computing the 33rd and 66th percentiles (which are 0.30 and 1.08 respectively)(Appendix E). Input parameters considered to have a low impact (relative to others tested) on the measured outputs have a mean percentage change (+/−) less than the 33rd percentile and are coloured in blue (Fig. 8), input parameters with a moderate effect have a percentage change (+/−) that falls between the 33rd and 66th percentile and are coloured in yellow. Those with a high effect on the output have a percentage change (+/−) greater than the 66th percentile of the data and are coloured in red.

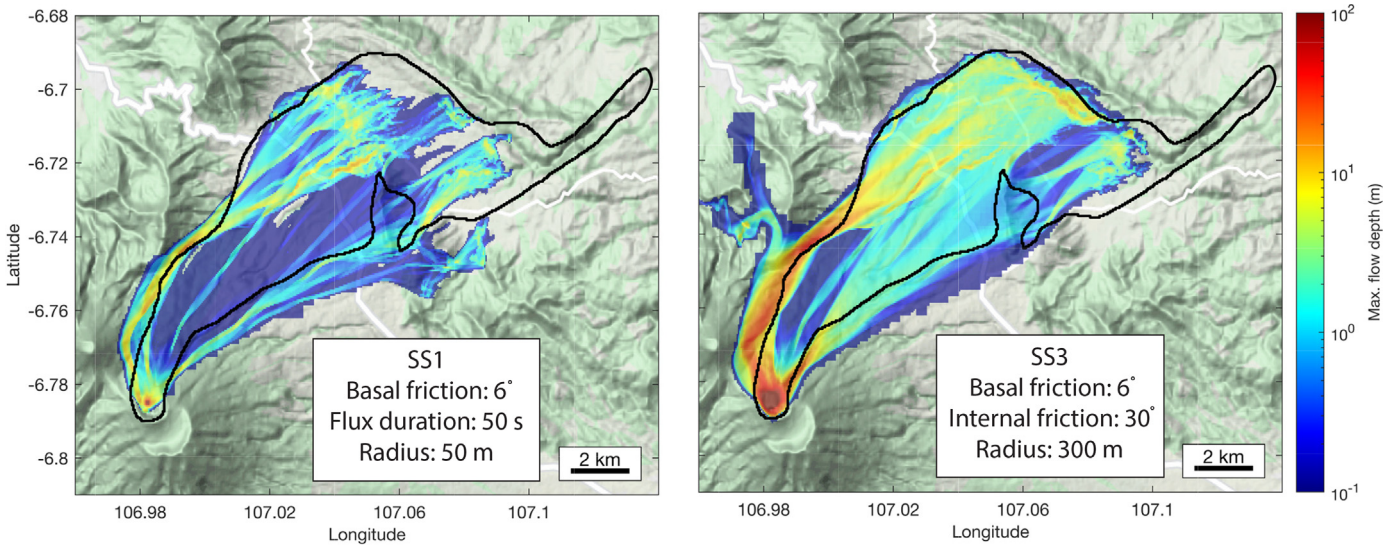

Fig. 6. Inundation areas for best fitting solutions for the 1.2 kyrs BP deposit, with the simulated maximum flow depth shown. The black line marks the extent of the field deposit (Belousov et al., 2015). SS1 is a flux type source from Gede crater; SS3 is a collapsing pile type source also from Gede crater.

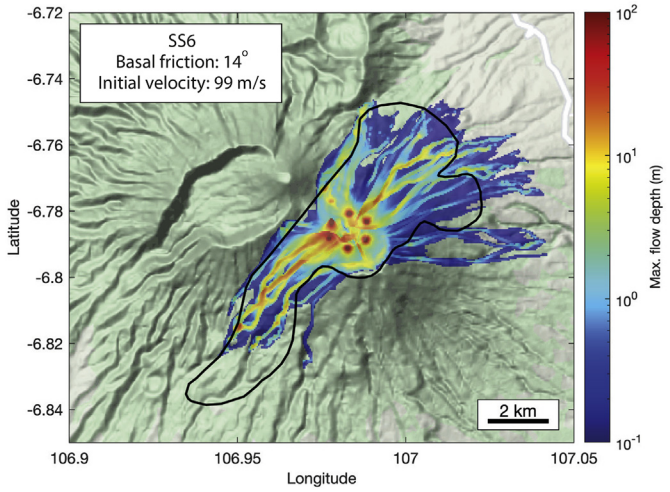

Fig. 7. Inundation area for the best fitting solution for the 1 kyrs BP deposit, with the simulated maximum flow depth shown. The black line marks the extent of the field deposit (Belousov et al., 2015). SS6 uses a multi-pile source type, which consisted of six piles of equal volume positioned radially around the Gede crater.

For both PDCs and all simulation subsets we found that the basal friction angle is by far the most influential input on runout (RO), and PDC footprint (Fig. 8), in agreement with previous studies (Sheridan et al., 2005; Dalbey, 2009, and Charbonnier and Gertisser, 2012). We found that the runout is most affected by changes to the basal friction angle in SS4 (simulations run for the Black-lapilli PDC). Sheridan et al. (2005) found a 54% reduction in PDC runout for a basal friction increase from 12° to 15° when simulating the 1963 avalanches at Mount Rainer. For comparison, increasing the basal friction angle value by the same amount for SS4 resulted in a 32% reduction in PDC runout. The varying sensitivity of simulation outputs across different volcanoes suggests that sensitivity testing should be carried out on a case-by-case basis and as a pre-requisite for any PDC hazard assessment.

For a pile collapse source (SS3) we tested Titan2D's sensitivity to the initial source location (for a fixed pile radius of 250 m and an internal friction angle of 25°), a parameter that has previously been considered important (Charbonnier and Gertisser, 2012). We found that moving the start location downslope in the direction that the PDC travelled (from the centre of Gede crater to the Wadon crater: 400 m) (Fig. 2b), resulted in a reduced PDC runout, and a smaller footprint. The greatest change in maximum PDC runout distance was 1.3 km while the average was 925 m. Such a disproportionate runout reduction in comparison to the change in start location suggests that the model is highly sensitive to this parameter (in agreement with Charbonnier and Gertisser, 2012). For Gede, this reduced flow mobility when flows are initiated from Wadon crater is likely controlled by topographic effects in addition to the reduction in momentum due to the lower elevation of the Wadon crater (elevation reduction ~200 m). Moving the start point downslope in this direction means that less material entered the Cipendawa and Ciguntur channels since the flow is no longer bifurcated by Sela ridge (Fig. 2b), a topographic high (and remnant crater wall) to the NE of the Gede crater, rising approximately 150 m and 70 m above the Ciwalen and Cipendawa channels respectively. This means that more material is deposited upstream in the Cikundul channel which is known to feature two localised basins (Section 5.1 – where the PDC meets the main channel and bends towards the NE, and at the Cibereum waterfall) and thus less material is available downstream, reducing the PDC length. By moving the start location towards the SW and into Ratu crater (Fig. 2b), material was able to overspill the present-day crater wall and travel towards the SW and the NE, instead of just the NE for other start locations.

5.3. Reconstructing 1948 tephra dispersion

Tephra falls that reached ~60 km to the SE and N during the 20 and 23 November 1948 explosions respectively, could not be reproduced using Tephra2 and the reported plume heights of these events (Petroeschevsky, 1952). However, with the aim of recreating the historical account, we chose to vary the eruption source parameters and wind conditions until we could reproduce tephra fall at the reported locations. By relaxing the parameters and wind conditions around the reported explosion times, we were able to reconstruct a plume for which tephra reached Gunung Patuha and Jakarta, albeit with a relatively low probability of occurrence.

Wind conditions across Java are highly seasonal. Analysis of 10 years of data centred on 1948 shows that throughout the dry season (April–October) the wind direction is predominantly towards the W up to heights of 10.5 km (Fig. 9). During the rainy season there is more variability in wind direction: at 5 km there is a roughly equal chance of wind blowing towards the E or W, although wind speeds are higher

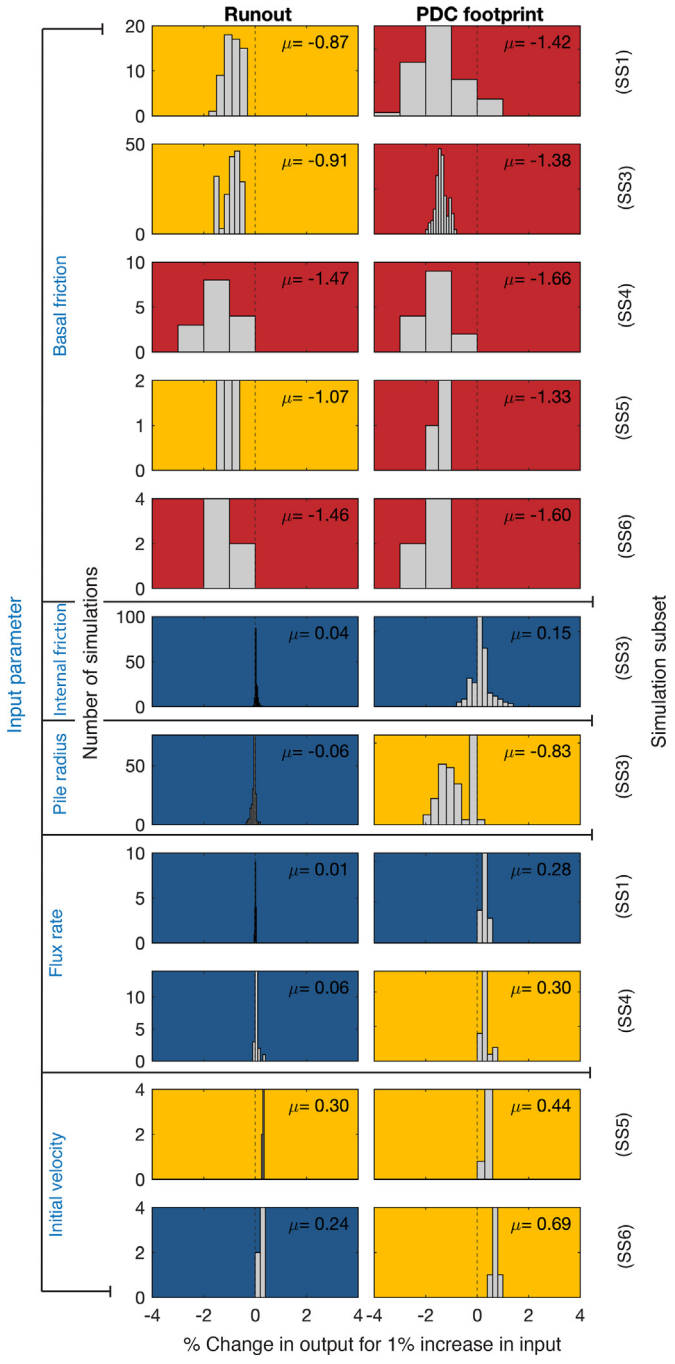

Fig. 8. Examining the sensitivity of model outputs (runout, and PDC footprint) to changes in model inputs (basal friction angle, internal friction angle, pile radius, flux rate and initial velocity). Plots show for each input parameter tested (blue text) the number of simulations (left y-axis) with a given percentage change in the output parameter for a 1% increase in the input (x-axis) for each simulation subset (right y-axis label). Positive values indicate that an increase in the input results in an increase in the output, while negative values suggest that an increase in the input results in a decrease in the output. Plot colour suggests relative sensitivity: high = red (> 66th percentile), moderate = yellow (33rd-66th percentile), low = blue (< 33rd percentile). The distribution of the total population of mean values is shown in Appendix E. Histogram bin widths were determined using 'Scotts rule' (Scott, 1979).

when blowing towards the E. At lower levels (3 km), the wind is more likely to blow towards the E in the rainy season. Analysis of the conditions during November, the month of the 1948 eruptions, shows that there is approximately a 2% probability that the wind would have been blowing towards Jakarta (N) at altitudes coinciding with the tephra injection height of explosions (~ 3000–5500 m.a.s.l. assuming a Beta plume model where $\alpha = \beta = 1$). There is also a similarly low probability of a SE wind direction (towards Gunung Patuha). Wind conditions at the time of the two explosions (Fig. 10) show that at heights coinciding with the tephra injection height, conditions during the 23 November eruption were close to the average conditions for the same month across the 10 year dataset, (Fig. 9) while on 20 November winds were blowing atypically towards the SW.

Results from each of the four scenarios modelled are summarised in Table 4. In Scenario 1, using the wind conditions at the time of the eruption and the reported column heights, there was a 0% probability of tephra reaching either Jakarta or Gunung Patuha. The same is true for Scenario 2, where 10 years of wind records were sampled from. Using the wind conditions at the time of the eruption, and an extended column height range between 1 and 15 km (a.s.l.) (Scenario 3) there was a 0% probability of exceeding the accumulation threshold, however a minor amount of tephra (< 0.1 kg/m^2) was deposited at Gunung Patuha and Jakarta with 29% and 0.2% probabilities respectively. If we relax the input ranges for both the wind conditions and the column height (Scenario 4), we found that it is possible for tephra to exceed the threshold accumulation, however the probability of this is very low with 0.2% at Gunung Patuha, and 0.03% at Jakarta. This suggests that the deposition of tephra fall at Jakarta and Gunung Patuha in 1948 was a rare occurrence. Fluctuations in the probability below 1% ($1/\sqrt{n}$) are non-informative and so we do not place any emphasis on the probability at Gunung Patuha being seemingly larger than that at Jakarta – both are very low probability occurrences.

The analysis of the eruption source parameters resulting in ground accumulations greater than 0.1 kg/m^2 at the two locations gives us an insight into the November 1948 explosions and the conditions that can cause tephra fallout in Indonesia's capital city (Fig. 11). In order to recreate a ground accumulation of ash ≥0.1 kg/m^2 at Gunung Patuha a minimum erupted mass of 3.12×10^9kg and a minimum plume height of 13 km above the vent is required, with winds blowing towards the site. For the same ground accumulation in Jakarta, a minimum erupted mass of 3.23×10^9kg and a minimum plume height of 13 km above the vent is needed. For both explosions, these plume heights are considerably larger than the ones reported (Petroeschevsky, 1952).

6. Discussion

6.1. Reconstructing PDC producing eruptions

PDC deposits are notoriously difficult to interpret in the field (Cronin et al., 2013), particularly when the deposits are old, and exposed to the high weathering rates associated with tropical regions. An example of this is provided by the contentious origins of the 2070 kyrs BP deposits at El Misti in Peru and whether they were generated by a PDC or lahar (see Cobeñas et al., 2012, 2014; and Harpel et al., 2011, 2013). One of the aims of this study was to further our understanding of the dynamics of our case study eruptions, and in the case of the 1.2 kyrs BP eruption we aimed to reduce the uncertainty surrounding the Lithic-rich PDC triggering mechanism. If the best fitting solutions were found using a flux source (SS1) then this might provide further evidence for a boiling over mechanism as suggested by Belousov et al. (2015), while if the best fitting solutions were found using a pile source type (SS3) then this would support a dome-collapse hypothesis suggested by the relatively low proportion of juvenile material. Unfortunately, the best fitting results were inconclusive in this sense, and both source types produced maximum best fitting similarity (S) values of 0.8, which makes it difficult to say that one PDC triggering mechanism is more likely than the other. However, inference from other model parameters can provide more insight.

The best fitting basal friction angle value for the Lithic-rich PDC was 6°, which is a relatively low value compared to PDCs simulated on other volcanoes (20°, Bursik et al. (2005); 20–28°, Rupp et al. (2006); 5–12°,

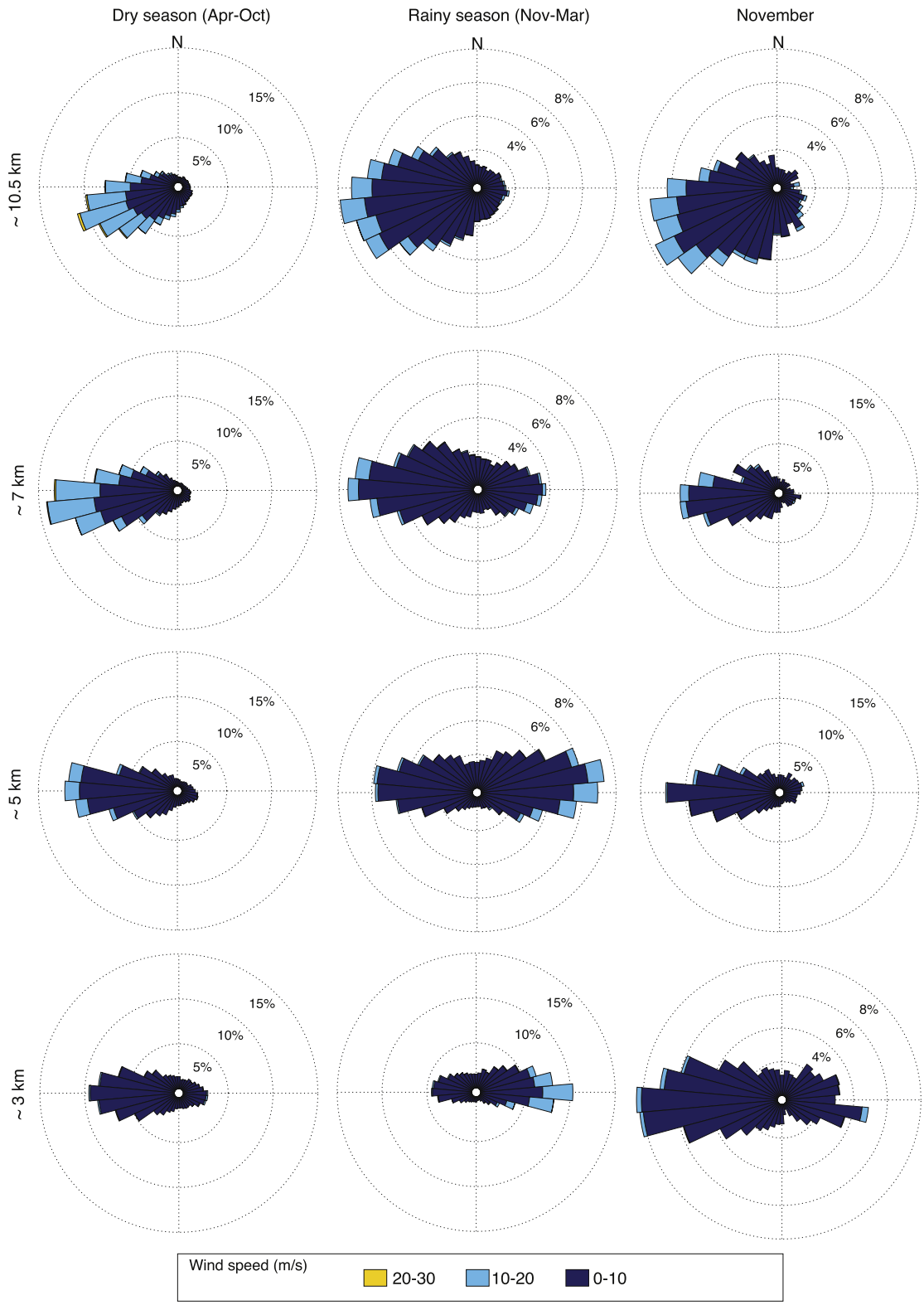

Fig. 9. Plots showing the wind conditions at Gede downloaded from the ECMWF ERA20C database for the period 1944–1953 at four different heights in the atmosphere (km above sea level). Wind roses show the probability of wind blowing towards a given direction during the dry season, rainy season, and in the month of November.

Hidayat et al. (2008); 15°, Murcia et al. (2010); 6–25°, Ogburn and Calder (2017)). Recreation of the Mixcun BAF at the Tacana Volcanic complex (Mexico-Guatemala) using Titan2D required a similarly low basal friction angle of 7° (Vázquez et al., 2019). The runout of the Lithic-rich PDC is comparable to the Mixcun BAF (although the volume of the Mixcun BAF is higher), which was triggered by a lateral blast (Macías et al., 2000). A low value was also required for reproduction of the 8 January 2010 PDC associated with Vulcanian activity at

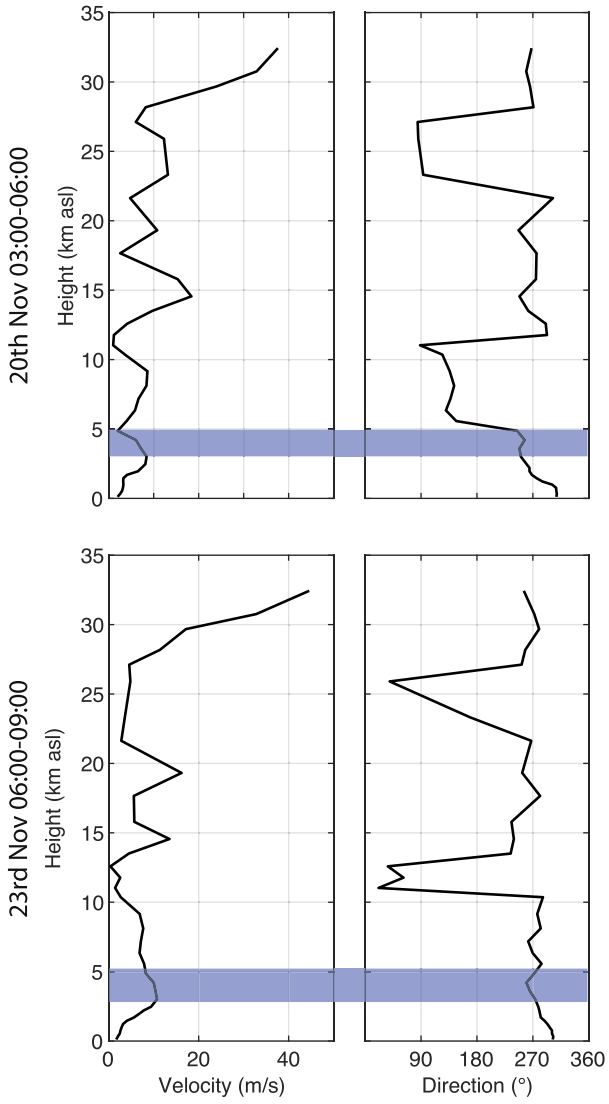

Fig. 10. Vertical wind profiles at the time of the two explosions, (20, 23 November 1948). Blue shaded areas mark the approximate tephra injection heights (assuming a uniform mass distribution within the plume). Tephra fall from the 20 November explosion was deposited close to Gunung Patuha 62 km SE of Gede, while tephra fall from the 23 November explosion was deposited in Jakarta 50 km N of Gede.

Soufrière Hills, Montserrat (Ogburn and Calder, 2017). Low values imply a highly mobile PDC, and for the Lithic-rich PDC at Gede it is unlikely that such runouts would have been produced by a dome-collapse event alone. We therefore suggest that, based on Titan2D simulations, the Lithic-rich PDC was generated by a non-buoyant column 'boiling over', as also suggested by Ogburn and Calder (2017) for the 8 January event at Montserrat. This interpretation is in agreement with the mechanism proposed by Belousov et al. (2015) for this PDC, based on field evidence alone. In the following paragraphs we further discuss the challenges that were presented when reconstructing these eruptions and provide alternative suggestions for the low basal friction angle required to recreate the Lithic-rich deposits.

Recreating the inundation areas of ancient PDCs is challenging primarily due to the lack of direct observations that can be used to initialise the modelling, and, to compare the outcomes with. The volume used to initialise Titan2D simulations was obtained from the stratigraphic study of Belousov et al. (2015) which was approximated from the PDC footprint and average deposit thickness, it is likely that this is an underestimation of the original deposited volume, which has been subjected to many years of reworking and weathering. Indeed, tropical weathering rates for solid andesitic rock can be up to 334 mm/kyrs (Dosseto et al., 2012), and are expected to be much higher for loose pyroclastic deposits. Uncertainty in the PDC volume also arises from our assumption that each of the four units of the 1.2 kyrs BP deposit equates to one flow, it's possible that one unit is either one pulse of a larger unsteady PDC, or the deposit was generated by several consecutive events. Several tests were run with a larger initial volume (both double and triple the value based on the deposits) and a more 'typical' basal friction angle of 12°. These tests showed that even when larger volumes were simulated, a higher basal friction angle was not able to reproduce the deposit. This makes it unlikely that an underestimation of the deposit volume is the reason for the low basal friction angle required, and also reiterates the model's sensitivity to this value. Furthermore, in the absence of observations for PDCs at Gede the initial source conditions for the modelling were taken from better studied analogues, this introduces an additional level of uncertainty delineated by the definition of an appropriate analogue. Regrettably, this situation is unavoidable when working on volcanoes with a short eruptive record.

The DEM is one of the main inputs for flow models operating over natural terrain, and the absence of a pre-flow DEM is one of the main areas of uncertainty in our modelling. Some studies have accounted for this by adapting a present-day DEM to represent the pre-PDC conditions (e.g. Charbonnier and Gertisser, 2009; Procter et al., 2010; Vázquez et al., 2019; Charbonnier et al., 2020), however this requires knowledge of the pre-flow topography and/or a detailed map of the deposit thickness (for example, Charbonnier et al. (2020) used 45 thickness data points), which is unavailable for Gede at this time. The low basal friction angle required to fit deposits, may also be related to the resolution of the DEM, and several authors have noted that for high resolution DEMs a lower basal friction angle is required to overcome irregularities in the topography (Sulpizio et al., 2010; Stefanescu et al., 2012). The Lithic-rich PDC has also been simulated with a 20 m DEM (Winson, 2016), resulting in no change to the best fitting value for the basal friction angle, which suggests that either: 1) the DEM resolution is not the reason for the low basal friction angle required or 2) the 20 m resolution used by Wilson et al. (1978) is not coarse enough to have a smoothing effect.

While Titan2D has been used to successfully recreate PDC deposits at many different volcanoes (e.g. Rupp et al., 2006; Procter et al., 2010; Sandri et al., 2014; Ogburn and Calder, 2017; Vázquez et al., 2019), Charbonnier et al. (2015) suggested that the Mohr-Coulomb frictional

Table 4
Probabilities for exceeding the 0.1 kg/m^2 tephra fall accumulation threshold at the localities reported by Petroeschevsky (1952) during the 1948 event. For each scenario 10,000 simulations were run.

Scenario	Wind	Col Ht	Gunung Patuha (62 km SE of Gede)		Jakarta (50 km N of Gede)	
			$P \geq 0.1$kg/m^2	$0 < P \leq 0.1$kg/m^2	P ≥ 0.1kg/m^2	0 < P ≤ 0.1kg/m^2
1	Fixed	Fixed	0% (n = 0)	0% (n = 0)	0% (n = 0)	0% (n = 0)
2	10 years	Fixed	0% (n = 0)	0% (n = 0)	0% (n = 0)	0% (n = 0)
3	Fixed	1–15 km	0% (n = 0)	29% (n = 2930)	0% (n = 0)	0.2% (n = 15)
4	10 years	1–15 km	0.2% (n = 20)	7% (n = 720)	0.03 (n = 3)	7% (n = 681)

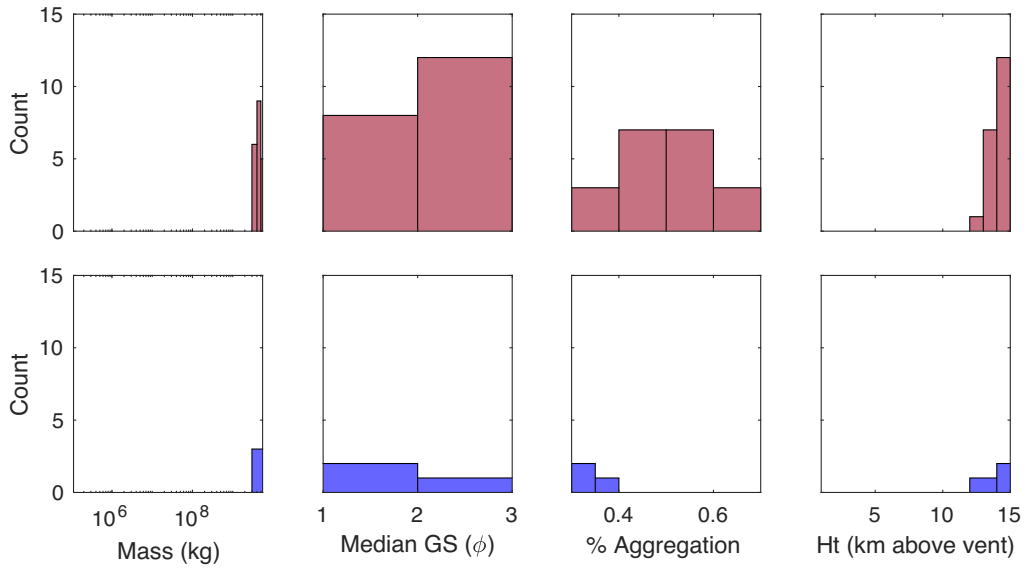

Fig. 11. Eruption source parameters contributing to the deposition of tephra greater than the critical threshold of 0.1 kg/m2 at Gunung Patuha (top), and Jakarta (bottom) for simulations sampling from 10 years of wind data, and a column height range of 1–15 km above the vent (Scenario 4).

model used in Titan2D may not be as suitable for recreating dilute PDCs or those resulting from a collapsing eruptive column. The low basal friction angle required to fit the Lithic-rich PDC at Gede may therefore represent that the flow was highly mobile, or that the DEM is problematic, or that the frictional model could not capture the dynamic PDC attributes well (e.g. thickness distribution and flow velocity). The distribution of deposits from BAFs at Tungurahua, 2006 (Kelfoun et al., 2009) and a boiling-over type PDC at Soufrière Hills, 2010 (Ogburn and Calder, 2017) could be accurately reproduced using Titan2D, but they were associated with unrealistically high velocities. A similar phenomenon can be seen in this study whereby the low basal friction angle and associated high flow velocity causes material to run-up against the topographic high towards the NE of Gede. Given these limitations we suggest that our best fitting model values be used as a first approximation in forecasting the inundation areas of future events, and careful attention should be paid to ensure that modelled flow velocities are realistic in each simulation. An alternative to the Coulomb frictional model applied in Titan2D is the two-phase model VolcFlow (Kelfoun, 2017), which uses a plastic rheology to describe flow behaviour. Future work might consider the use of a more advanced model such as this one to reproduce this flow. However, the use of this type of numerical model requires a greater computational expense, as well as a larger number of inputs that would need to be approximated from analogues.

The methodology that we have presented provides a structured and quantitative solution for assessing the goodness of fit between field deposits and simulated deposits. In this work, we used a measure of two parameters, combining the runout and the PDC footprint with equal weighting for our comparison, however if more additional robust information is available, for example average flow thickness, thickness measurements at point locations, or measurements of PDC velocity, then this could be incorporated into the similarity value (S) and weighted accordingly. The value of considering goodness of fit across multiple parameters, is that the best fitting parameters used for future hazard assessment can be guided by the most relevant parameter to reproduce. For example, the maximum runout or PDC footprint may be more important for evacuation planning than the average thickness, but the thickness may be the most relevant parameter for reconstruction or rehabilitation planning. The choice of weighting is subjective, however we suggest that its quantification should reflect both the relative importance of reproducing the specific parameter and the confidence placed in the field data. For example quarrying might mean that parts of the field deposit are missing and we might choose to down-weight the PDC footprint metric in the calculation of S. Alternative weighting schemes and their impacts on the results are provided in Appendix F.

6.1.1. Implications for forecasting future PDC hazards at Gede

While using the present-day topography is one of the key limitations in this work, it has given us a preliminary insight into future PDC hazard at Gede. We suggest that Gede is likely to experience future PDCs resulting from a range of mechanisms, including partial or full column-collapse, boiling over of a non-buoyant column, and dense BAFs resulting from collapse of a lava dome. Due to the topography of the crater (the north-wards sloping summit, along with the northward opening amphitheatre and steep S crater wall), future lava dome extrusion and collapse is likely to be northerly directed unless the summit topography is altered. We also note the importance of Sela ridge in controlling the distribution of future PDCs. If a future flow should initiate towards the north of the summit area (Wadon crater), the majority of material would likely enter the Cikundul channel; however, if a flow should initiate farther south within the Gede crater, then we can expect thicker deposits in the Cipendawa and Ciguntur channels which lie closer to the populated area of Cibodas (Fig. 1). This highlights the importance of monitoring the crater region during lava dome extrusion to assess the directionality and therefore potential collapse locations. Our simulations of collapsing piles with heights > ~600 m resulted in inundation of the SW flank in addition to the NE, suggesting that a future fountain collapse (effective column collapse heights >600 m) under a no-wind scenario may inundate multiple flanks. The best fitting parameter values acquired through this study can be used to further investigate future PDC hazard, quantifying their spatial extent and likelihood. Given the lack of data available regarding past eruptions, and the uncertainties inherent in any future estimation, we would recommend using a probabilistic approach. It is also important to reiterate that Titan2D should only be used to model the dense undercurrent of PDCs, not the dilute surge layer which is capable of travelling beyond this. For this matter, a buffer zone based on empirical data could be used to extend this (Widiwijayanti et al., 2008) or a more complex two-phase model such as VolcFlow (Kelfoun, 2017) might be employed for this purpose.

6.2. Reconstructing the 1948 tephra dispersion

Reproducing the reported tephra fall at Jakarta and Gunung Patuha was not possible using the information sourced from Petroeschevsky (1952). We propose a number of potential reasons for this. Firstly, we introduce the possibility that Petroeschevsky (1952) may have been inaccurate – this would have implications for evaluating the range of potential future eruptions, and therefore the related hazards. The report of Petroeschevsky (1952) was used to source plume heights, explosion times and fall locations. It's possible that the plume heights were incorrectly estimated or recorded, or the time of the explosions was miscommunicated. The discrepancy between the reported plume heights (~2, 2.5 km) and the heights obtained in this work (~13 km) however is significant, and such an underestimation seems unlikely. Furthermore, tephra fall deposits at Gede are restricted to the flanks of the volcano (Bear-Crozier et al., 2012; Belousov et al., 2015) and if Gede did erupt a 13 km plume in 1948, we would expect there to be more evidence of this in the geological and historical record. An alternative suggestion related to the accuracy of the report, is that the reported tephra fall did not originate from Gede volcano, however there were no sizeable eruptions recorded in the region at this time. Secondly, we consider that the spatial, and/or temporal resolution of the meteorological data may be insufficient to capture small changes in the wind conditions. Dispersion from low plumes such as those considered in this study occurs primarily in the lower troposphere, where wind conditions are influenced by topography and are highly variable spatially and temporally (Scollo et al., 2008; Bonadonna and Costa, 2013). Finally, we note that two-dimensional tephra dispersal models like Tephra2 are not well suited to the transport of fine tephra particles due to the omission of vertical wind velocity, since fine particles often have settling velocities that are lower than the vertical velocity (Scollo et al., 2008). Phreatomagmatic eruptions, which are known to have occurred at Gede, typically produce finer tephra fractions (Rust and Cashman, 2011) and so it may be that a more sophisticated (and data- and computing intensive) three-dimensional model is required to capture the transport of fine tephra.

In our modelling the input parameters that could not be sourced from Petroeschevsky (1952) were taken from appropriate analogues, for example the TGSD was acquired from Soufrière St Vincent (Brazier et al., 1982), the Tephra2 empirical parameters used (diffusion coefficient, and fall time threshold) were the best fitting inversion values for Fuego volcano (Guatemala) (Biass et al., 2016b), and the plume model was the best fit for explosions at Soufrière Hills Volcano, Montserrat (Bonadonna et al., 2002). The TGSD used is thus potentially depleted in fines, since the eruption occurred on an island and the finer tephra fraction was likely deposited in the ocean. To check the impact of this we tested an arbitrarily fine TGSD, but found there to be minimal difference in the resulting tephra accumulation at the two locations, suggesting that the TGSD used for our analysis is appropriate or at least does not strongly influence the results. In Tephra2, particle diffusion is treated differently for coarse and fine particles; for coarse particles diffusion is linear, while for fine particles a power-law relationship is adopted (Bonadonna et al., 2005). This is controlled in the modelling by two empirical values; the diffusion coefficient describes linear diffusion, while the fall time threshold (FTT) controls the transition between regimes. A higher FTT means that more particles are modelled with linear diffusion, which is likely to result in increased deposition closer to the vent. This was taken into account when choosing a suitable analogue; however, as with the TGSD, we tested an arbitrarily low FTT and found there to be minimal changes to the resulting tephra accumulation. These findings support our choice of analogue values and the forementioned potential reasons for our inability to recreate the reported tephra fall.

Analysis of the 10 year wind dataset has shown that the probability of wind blowing in a direction that is favourable to deposition in Indonesia's capital city Jakarta is very low (Fig. 9). This suggests that future VEI2 sized eruptions at Gede are unlikely to result in the deposition of a noticeable quantity of tephra in Jakarta, although a larger eruption (upwards of VEI 3) with a column height in excess of 13 km has the potential to do so. Whilst the probability of a wind direction favourable for deposition at Jakarta is low, it is not impossible, highlighting the importance of probabilistic strategies in forecasting future tephra fall hazard, since considering only the most likely wind scenario would result in omission of such a high impact event. Throughout the dry season the predominance of westerly winds suggests that a future tephra fall hazard will be concentrated towards the west for small eruption columns with plume heights less than ~7.5 km. During the rainy season, both the W and E directions are likely to be impacted by tephra fall. Future tephra hazard assessment studies will enable further quantification of this.

7. Concluding remarks

In this work we reconstructed three historic eruptions at Gede volcano by using the numerical models Titan2D and Tephra2 to recreate PDC field deposits and a historical account of tephra fall. Subsequent examination of the best fitting model solutions allowed for a discussion on some of the challenges associated with reconstructing eruptions at a data limited volcano, and allowed us to make a number of inferences about the eruptions that produced the deposits.

Reconstructing eruptions when faced with few or uncertain data is a challenging, but necessary, step towards volcanic hazard assessment. Some of the main challenges include: a lack of direct observations that can be used as hazard model inputs; high weathering rates that make geological deposits difficult to interpret or mean that portions may not be preserved; and uncertainty surrounding the accuracy of historical accounts.

In light of these uncertainties, using a deliberately broad range of inputs within a stochastic modelling approach provides a simple solution to narrowing down the best fitting parameter space. We developed a flexible and quantitative approach to assessing the goodness of fit between simulation outputs and field observations. The method is capable of incorporating any number of metrics used to judge fit (for PDCs we used runout and PDC footprint) and weighting them in accordance with the confidence placed on their accuracy. Approaches such as this are important for robustly and objectively assessing the fit between model values and field data.

This methodology was applied to recreate the Lithic-rich and Black-lapilli PDCs produced by eruptions at Gede volcano 1.2 kyrs BP and 1 kyrs BP respectively. Multiple modelling approaches were used to recreate the field deposits, showing that the highly mobile Lithic-rich PDC could be reproduced using either a flux (representing a non-buoyant column boiling over) or a collapsing pile (representing gravitational dome-collapse) source type. This information was used in conjunction with past stratigraphic work to suggest that the PDC was likely generated by a boiling over type triggering mechanism, which also explains the high mobility. For the Black-lapilli PDC; fountain collapse from a relatively low 2.5 km plume (collapse height 250 m) is suggested as the generation mechanism. A model source consisting of multiple piles positioned radially around the crater provided the best fit.

Reproduction of the tephra falls of 20, 23 November 1948 using the column heights reported in Petroeschevsky (1952), and the meteorological conditions at the time was not possible. This may be related to inaccuracies in the historical report and/or the limitations of Tephra2 and/or the meteorological data in simulating small volume eruptions with low plume heights. The meteorological conditions in the region are not conducive to dispersing tephra from a small Vulcanian eruption at Gede towards the capital city of Jakarta. Assuming a plume height of 2.5 km above the vent (as reported for the 23 November 1948, Petroeschevsky, 1952), a northerly wind direction has a probability of ~2%. For the model to produce noticeable accumulation of tephra in

Jakarta a minimum plume height of 13 km above the vent, and a minimum erupted mass of 3.23×10^9 kg is required.

Gede is the world's most populous volcano and ancient PDC deposits underlie the densely populated town of Cibodas in the NE. With a short historical record, it is critical that as much information as possible is extracted from the data that we do have for past eruptions. This study presents an important first step towards hazard and risk assessment for Gede. Future work should make use of the Titan2D sensitivity testing results, along with the best fitting model values obtained for the PDC field deposits; using these to build statistical distributions of the most important model inputs, which in turn can be sampled and used for running probabilistic scenarios forecasting the spatial extent of future PDC's. We recommend a probabilistic approach for simulating the spatial extent of PDCs, tephra fall, lahars, and volcanic ballistic projectiles. Where information is lacking for Gede, eruption scenarios and model input values should be sourced from analogue volcanoes.

Author contributions

EMT, SFJ, and AW conceived the study. EMT and SFJ developed the methodology, with support and expertise regarding Gede volcano from CW, HG, NH, NK, WB, and HT. EMT carried out Titan2D and Tephra2 modelling, with input from CW and AW. EMT, SFJ, and CW analysed the results of the PDC modelling, and EMT and SFJ analysed the results for tephra. EMT wrote the original draft of the manuscript with all authors editing and reviewing the draft prior to submission.

Declaration of Competing Interest

The authors declare that they have no known competing financial interests or personal relationships that could have appeared to influence the work reported in this paper.

Acknowledgements

This research was supported by the Earth Observatory of Singapore via its funding from the National Research Foundation Singapore and the Singapore Ministry of Education under the Research Centres of Excellence initiative. Early parts of this work were also supported by Agency for Science, Technology and Research (A*STAR). This work comprises EOS contribution number 348. We would like to thank Fidel Costa and Chris Newhall for their long-standing support of hazard assessment studies at Gede volcano and also Eliza Calder for her insights and feedback on early efforts to model PDCs at Gede. We are grateful to Alexander and Marina Belousov and Adele Bear-Crozier for information regarding field studies in the area. We would also like to thank Samantha Engwell for comments on the manuscript along with Rosario Vázquez and Ben Clarke for their insightful reviews.

Appendix A. Supplementary data

Supplementary data to this article can be found online at https://doi.org/10.1016/j.jvolgeores.2021.107325.

References

Aryanti, E., Nugraha, A.D., Basuki, A., Triastuty, H., 2018. 3D seismic tomography Vp, Vs and Vp/Vs ratio beneath Gede Volcano, West Java, Indonesia. AIP Conference Proceedings, 1987(July) https://doi.org/10.1063/1.5047331.

Bear-Crozier, A.N., Kartadinata, N., Heriwaseso, A., Nielsen, O., 2012. Development of python-FALL3D: a modified procedure for modelling volcanic ash dispersal in the Asia-Pacific region. Nat. Hazards 64, 821–838. https://doi.org/10.1007/s11069-012-0273-7.

Belousov, A., Belousova, M., Krimer, D., Costa, F., Prambada, O., Zaennudin, A., 2015. Volcaniclastic stratigraphy of Gede Volcano, West Java, Indonesia: how it erupted and when. J. Volcanol. Geotherm. Res. 301, 238–252. https://doi.org/10.1016/j.jvolgeores.2015.05.018.

Beven, K.J., Aspinall, W.P., Bates, P.D., Borgomeo, E., Goda, K., Hall, J.W., Page, T., Phillips, J.C., Simpson, M., Smith, P.J., Wagener, T., Watson, M., 2018. Epistemic uncertainties and natural hazard risk assessment-Part 2: what should constitute good practice? Nat. Hazards Earth Syst. Sci. 18, 2769–2783. https://doi.org/10.5194/nhess-2017-251.

Biass, S., Bonadonna, C., Connor, L., Connor, C., 2016a. TephraProb: a Matlab package for probabilistic hazard assessments of tephra fallout. J. Appl. Volcanol. 5, 1–16. https://doi.org/10.1186/s13617-016-0050-5.

Biass, S., Bonadonna, C., di Traglia, F., Pistolesi, M., Rosi, M., Lestuzzi, P., 2016b. Probabilistic evaluation of the physical impact of future tephra fallout events for the Island of Vulcano, Italy. Bull. Volcanol. 78 (37), 1–22. https://doi.org/10.1007/s00445-016-1028-1.

Biass, S., Todde, A., Cioni, R., Pistolesi, M., Geshi, N., Bonadonna, C., 2017. Potential impacts of tephra fallout from a large-scale explosive eruption at Sakurajima volcano, Japan. Bull. Volcanol. 79 (73). https://doi.org/10.1007/s00445-017-1153-5.

Bonadonna, C., Costa, A., 2013. Modeling tephra sedimentation from volcanic plumes. In: Fagents, S., Gregg, T., Lopes, R. (Eds.), Modeling Volcanic Processes: The Physics and Mathematics of Volcanism. Cambridge University Press, Cambridge, pp. 173–202 https://doi.org/10.1017/CBO9781139021562.009.

Bonadonna, C., Macedonio, G., Sparks, R.S.J., 2002. Numerical modelling of tephra fallout associated with dome collapses and Vulcanian explosions: application to hazard assessment on Montserrat. Geol. Soc. Mem. 21, 517–537. https://doi.org/10.1144/GSL.MEM.2002.021.01.23.

Bonadonna, C., Connor, C.B., Houghton, B.F., Connor, L., Byrne, M., Laing, A., Hincks, T., 2005. Probabilistic modeling of tephra dispersal: Hazard assessment of a multiphase rhyolitic eruption at Tarawera, New Zealand. J. Geophys. Res. Solid Earth 110 (3), 1–21. https://doi.org/10.1029/2003JB002896.

Bonasia, R., Macedonio, G., Costa, A., Mele, D., Sulpizio, R., 2010. Numerical inversion and analysis of tephra fallout deposits from the 472 AD sub-Plinian eruption at Vesuvius (Italy) through a new best-fit procedure. J. Volcanol. Geotherm. Res. 189 (3–4), 238–246. https://doi.org/10.1016/j.jvolgeores.2009.11.009.

Branney, M.J., Kokelaar, P., 2002. Pyroclastic Density Currents and the Sedimentation of Ignimbrites. The Geological Society, London.

Brazier, S., Davis, A.N., Sigurdsson, H., Sparks, R.S.J., 1982. Fall-out and deposition of volcanic ash during the 1979 explosive eruption of the Soufriere of St. Vincent. J. Volcanol. Geotherm. Res. 14, 335–359. https://doi.org/10.1016/0377-0273(82)90069-5.

Brown, S.K., Auker, M.R., Sparks, R.S.J., 2015. Populations around holocene volcanoes and development of a population exposure index. Global Volcanic Hazards and Risk. Cambridge University Press, pp. 223–232 https://doi.org/10.1017/CBO9781316276273.006.

Bursik, M., Patra, A., Pitman, E.B., Nichita, C., Macias, J.L., Saucedo, R., Girina, O., 2005. Advances in studies of dense volcanic granular flows. Rep. Prog. Phys. 68, 271–301. https://doi.org/10.1088/0034-4885/68/2/R01.

Calder, E.S., Cole, P.D., Dade, W.B., Druitt, T.H., Hoblitt, R.P., Hupert, H.E., Ritchie, L., Sparks, R.S., Young, S.R., 1999. Mobility of pyroclastic flows and surges at the Soufrière Hills volcano, Montserrat. Geophys. Res. Lett. 26, 537–554.

Charbonnier, S.J., Gertisser, R., 2009. Numerical simulations of block-and-ash flows using the Titan2D PDC model: examples from the 2006 eruption of Merapi Volcano, Java, Indonesia. Bull. Volcanol. 71, 953–959. https://doi.org/10.1007/s00445-009-0299-1.

Charbonnier, S.J., Gertisser, R., 2012. Evaluation of geophysical mass flow models using the 2006 block-and-ash PDCs of Merapi Volcano, Java, Indonesia: towards a short-term hazard assessment tool. J. Volcanol. Geotherm. Res. 231–232, 87–108. https://doi.org/10.1016/j.jvolgeores.2012.02.015.

Charbonnier, S.J., Germa, A., Connor, C.B., Gertisser, R., Preece, K., Komorowski, J.C., Lavigne, F., Dixon, T., Connor, L., 2013. Evaluation of the impact of the 2010 pyroclastic density currents at Merapi volcano from high-resolution satellite imagery, field investigations and numerical simulations. J. Volcanol. Geotherm. Res. 261, 295–315. https://doi.org/10.1016/j.jvolgeores.2012.12.021.

Charbonnier, S.J., Palma, J.L., Ogburn, S., 2015. Aplicación de modelos numéricos de "aguas someras" para el análisis de peligros de flujos volcánicos: El caso de Titan2D y volcán Turrialba (Costa Rica). Rev. Geol. Am. Central 52, 107–128. https://doi.org/10.15517/rgac.v0i52.19021.

Charbonnier, S.J., Connor, C.B., Connor, L.J., Sheridan, M.F., Oliva Hernández, J.P., Richardson, J.A., 2018. Modeling the October 2005 lahars at Panabaj (Guatemala). Bull. Volcanol. 80 (4). https://doi.org/10.1007/s00445-017-1169-x.

Charbonnier, S.J., Thouret, J.C., Gueugneau, V., Constantinescu, R., 2020. New insights into the 2070calyrBP Pyroclastic Currents at El Misti Volcano (Peru) from field investigations, satellite imagery and probabilistic modeling. Front. Earth Sci. 8, 1–20. https://doi.org/10.3389/feart.2020.557788.

Cobeñas, G., Thouret, J.-C., Bonadonna, C., Boivin, P., 2012. The c.2030yr BPPlinian eruption of El Misti volcano, Peru: eruption dynamics and hazard implications. J. Volcanol. Geotherm. Res. 241-242, 105–120. https://doi.org/10.1016/j.jvolgeores.2012.06.006.

Cobeñas, G., Thouret, J.C., Bonadonna, C., Boivin, P., 2014. Reply to comment on: "Cobeñas, G., Thouret, J.-C., Bonadonna, C., Boivin, P., 2012. The c.2030yr BP Plinian eruption of El Misti volcano, Peru: Eruption dynamics and hazard implications. Journal of Volcanology and Geothermal Research 241–242, 105–120." by Harpel et al., JVGR 2013. J. Volcanol. Geotherm. Res. 275, 103–113. https://doi.org/10.1016/j.jvolgeores.2014.02.014.

Connor, L.J., Connor, C.B., 2006. Inversion is the key to dispersion: Understanding eruption dynamics by inverting tephra fallout. In: Mader, H., Cole, S., Connor, C.B., Connor, L.G. (Eds.), Statistics in Volcanology. Geological Society, London, pp. 231–242.

Constantinescu, R., Thouret, J.C., Irimuş, I.A., 2011. Computer modeling as tool for volcanic hazards assessment: an example of pyroclastic PDC modeling at el misti volcano, Southern Peru. Geogr. Tech. 2, 1–14.

Cronin, S.J., Lube, G., Dayudi, D.S., Sumarti, S., Subrandiyo, S., Surono, 2013. Insights into the October-November 2010 Gunung Merapi eruption (Central Java, Indonesia) from the stratigraphy, volume and characteristics of its pyroclastic deposits. J. Volcanol. Geotherm. Res. 261, 244–259. https://doi.org/10.1016/j.jvolgeores.2013.01.005.

Dalbey, K., 2009. Predictive Simulation and Model Based Hazard Maps of Geophysical Mass PDCs. PhD thesis. State University New York, Buffalo.
Dosseto, A., Buss, H.L., Suresh, P.O., 2012. Rapid regolith formation over volcanic bedrock and implications for landscape evolution. Earth Planet. Sci. Lett. 337–338, 47–55. https://doi.org/10.1016/j.epsl.2012.05.008.
Druitt, T.H., Young, S.R., Baptie, B., Bonadonna, C., Calder, E.S., Clarke, A.B., Cole, P.D., Harford, C.L., Herd, R.A., Luckett, R., Ryan, G., Voight, B., 2002. Episodes of cyclic Vulcanian explosive activity with fountain collapse at Soufrière Hills Volcano, Montserrat. Geol. Soc. Lond. Mem. 21, 281–306. https://doi.org/10.1144/GSL.MEM.2002.021.01.13.
Geospatial Information Agency, 2018. DEMNAS. http://tides.big.go.id/DEMNAS/.
Global Volcanism Program, 2013. Gede-Pangrango (263063). In: Venzke, E. (Ed.), Volcanoes of the World. Vol. v. 4.8.8. Smithsonian Institution https://doi.org/10.5479/si.GVP. VOTW4-2013.
Harpel, C., De Silva, S., Salas, G., 2011. The 2 ka Eruption of Misti Volcano, Southern Peru—the Most recent Plinian Eruption of Arequipa's Iconic Volcano. Spec. Pap. Geol. Soc. Am. 484, 1–72. https://doi.org/10.1130/2011.2484.
Hadisantono, R.D., Abdurachman, A., Martono, A., Sumpena, A.D., Wahyu, S., Santoso, M.S., 2008. Volcanic Hazard Map of Gede Volcano, West Java Province. Center for Volcanology and Geological Hazard Mitigation, Bandung Scale 1:50,000.
Harpel, C., da Silva, S., Salas, G., 2013. Comment on: "Cobeñas, G., Thouret, J.-C., Bonadonna, C., Boivin, P., 2012. The c.2030 yr BP Plinian eruption of El Misti volcano, Peru: eruption dynamics and hazard implications. Journal of Volcanology and Geothermal Research 241–242, 105–120". J. Volcanol. Geotherm. Res. 265, 94–101. https://doi.org/10.1016/j.jvolgeores.2014.02.014.
Heim, A., 1932. Bergsturz und Menschenleben. Fretz and Wasmuth, Zurich 218p.
Heinrich, P., Boudon, G., Komorowski, J.C., Sparks, R.S.J., Herd, R., Voight, B., 2001. Numerical simulation of the December 1997 debris avalanche in Montserrat, Lesser Antilles. Geophys. Res. Lett. 28 (13), 2529–2532.
Hidayat, D., Widiwijayanti, C., Voight, B., Patra, A.K., Pitman, E.B., 2008. TITAN2D Based Modeling of Dome-Collapse Pyroclastic Flows for Crisis Assessments on Montserrat. IAVCEI General Assembly, Reykjavik, Iceland.
Hidayat, D., Basuki, A., Nurrokhman, N., Kristianto, K., Taisne, B., 2019. Volcanic structure under Gede, West Java, Indonesia, results from three-dimensional local earthquake tomography and small long-period earthquake analysis. EGU General Assembly, Vienna, Austria, 7–12 April.
Iverson, R.M., Schilling, S.P., Vallance, J.W., 1998. Objective delineation of lahar-inundation hazard zones. Bull. Geol. Soc. Am. 110, 972–984. https://doi.org/10.1130/0016-7606(1998)110<0972:ODOLIH>2.3.CO;2.
Jenkins, S.F., Phua, M., Warren, J.F., Biass, S., Bouvet de Maisonneuve, C., 2020. Reconstructing Eruptions from Historical Accounts: Makaturing c. 1765, Philippines. J. Volcanol. Geotherm. Res. 404, 107022. https://doi.org/10.1016/j.jvolgeores.2020.107022 0377-0273.
Johnston, E.N., Phillips, J.C., Bonadonna, C., andd Watson, I. M., 2012. Reconstructing the tephra dispersal pattern from the Bronze Age eruption of Santorini using an advection-diffusion model. Bull. Volcanol. 74 (6), 1485–1507. https://doi.org/10.1007/s00445-012-0609-x.
Kelfoun, K., 2017. A two-layer depth-averaged model for both the dilute and the concentrated parts of pyroclastic currents. J. Geophys. Res. Solid Earth 122 (6), 4293–4311. https://doi.org/10.1002/2017JB014013.
Kelfoun, K., Samaniego, P., Palacios, P., Barba, D., 2009. Testing the suitability of frictional behaviour for pyroclastic flow simulation by comparison with a well-constrained eruption at Tungurahua volcano (Ecuador). Bull. Volcanol. 71 (9), 1057–1075. https://doi.org/10.1007/s00445-009-0286-6.
Kilgour, G., Gates, S., Kennedy, B., Farquhar, A., McSporran, A., Asher, C., 2019. Phreatic eruption dynamics derived from deposit analysis: a case study from a small, phreatic eruption from Whakāri/White Island, New Zealand. Earth Planets Space 71, 36. https://doi.org/10.1186/s40623-019-1008-8.
Kubanek, J., Richardson, J.A., Charbonnier, S.J., Connor, L.J., 2015. Lava flow mapping and volume calculations for the 2012–2013 Tolbachik, Kamchatka, fissure eruption using bistatic TanDEM-X InSAR. Bull. Volcanol. 77, 1–13. https://doi.org/10.1007/s00445-015-0989-9.
Legros, F., 2002. The mobility of long-runout landslides. Eng. Geol. 63 (3–4), 301–331. https://doi.org/10.1016/S0013-7952(01)00090-4.
Macías, J.L., Espíndola, J.M., García-Palomo, A., Scott, K.M., Hughes, S., Mora, J.C., 2000. Late Holocene Peléan-style eruption at Tacaná volcano, Mexico and Guatemala: past, present, and future hazards. Geol. Soc. Am. Bull. 112 (8), 1234–1249.
Macías, J.L., Capra, L., Arce, J.L., Espíndola, J.M., García-Palomo, A., Sheridan, M.F., 2008. Hazard map of El Chichón volcano, Chiapas, México: constraints posed by eruptive history and computer simulations. J. Volcanol. Geotherm. Res. 175 (4), 444–458. https://doi.org/10.1016/j.jvolgeores.2008.02.023.
Magill, C., Wilson, T., Okada, T., 2013. Observations of tephra fall impacts from the 2011 Shinmoedake eruption, Japan. Earth Planets Space 65, 677–698. https://doi.org/10.5047/eps.2013.05.010.
Murcia, H.F., Sheridan, M.F., Macías, J.L., Cortés, G.P., 2010. TITAN2D simulations of pyroclastic flows at Cerro Machín Volcano, Colombia: hazard implications. J. S. Am. Earth Sci. 29, 161–170. https://doi.org/10.1016/j.jsames.2009.09.005.
Newhall, C.G., Self, S., 1982. The volcanic explosivity index (VEI) an estimate of explosive magnitude for historical volcanism. J. Geophys. Res. 87, 1231–1238. https://doi.org/10.1029/JC087iC02p01231.
Nugraha, A.K., Maryanto, S., Triastuty, H., 2017. Hypocenter Determination and Clustering of Volcano-Tectonic Earthquakes in Gede Volcano 2015. J. Neutrino 9 (2), 46–52. https://doi.org/10.18860/neu.v9i2.4103.
Ogburn, S., 2012. Flowdat:Mass flowdatabase v2.2. On Vhub at. https://vhub.org/groups/massflowdatabase.
Ogburn, S.E., Calder, E.S., 2017. The relative effectiveness of empirical and physical models for simulating the dense undercurrent of pyroclastic flows under different emplacement conditions. Front. Earth Sci. 5, 83. https://doi.org/10.3389/feart.2017.00083.
Paone, A., Yun, S.-H., 2016. Pyroclastic density current hazards at the baekdusan volcano, Korea: analyses of several scenarios from a small-case to the worst-case colossal eruption. Updates in Volcanology-From Volcano Modelling to Volcano Geology. InTech press, London, UK.
Patra, A.K., Bauer, A.C., Nichita, C.C., Pitman, E.B., Sheridan, M.F., Bursik, M., Rupp, B., Webber, A., Stinton, A.J., Namikawa, L.M., Renschler, C.S., 2005. Parallel adaptive numerical simulation of dry avalanches over natural terrain. J. Volcanol. Geotherm. Res. 139 (1–2), 1–21. https://doi.org/10.1016/j.jvolgeores.2004.06.014.
Petroeschevsky, W.A., 1952. The volcanic activity in Indonesia during the period 1942-1948, Berita, Gunung Berapi 1:17-30; 3-4:931.
Poli, P., Hersbach, H., Dee, D.P., Berrisford, P., Simmons, A.J., Vitart, F., Laloyaux, P., Tan, D.G.H., Peubey, C., Thépaut, J.N., Trémolet, Y., Hólm, E.V., Bonavita, M., Isaksen, L., Fisher, M., 2016. ERA-20C: an atmospheric reanalysis of the twentieth century. J. Clim. 29 (11), 4083–4097. https://doi.org/10.1175/JCLI-D-15-0556.1.
Procter, J.N., Cronin, S.J., Platz, T., Patra, A., Dalbey, K., Sheridan, M., Neall, V., 2010. Mapping block-and-ash flow hazards based on Titan 2D simulations: a case study from Mt. Taranaki, NZ. Nat. Hazards 53, 483–501. https://doi.org/10.1007/s11069-009-9440-x.
Rose, A.N., McKee, J.J., Urban, M.L., Bright, E.A., Sims, K.M., 2019. LandScan 2018. https://landscan.ornl.gov/.
Rupp, B., Bursik, M., Namikawa, L., Webb, A., Patra, A.K., Saucedo, R., Macías, J.L., Renschler, C., 2006. Computational modeling of the 1991 block and ash flows at Colima Volcano, México. Spec. Pap. Geol. Soc. Am. 402, 237–252. https://doi.org/10.1130/2006.2402(11).
Rust, A.C., Cashman, K.V., 2011. Permeability controls on expansion and size distributions of pyroclasts. J. Geophys. Res. Solid Earth 116 (11), 1–17. https://doi.org/10.1029/2011JB008494.
Rutarindwa, R., Spiller, E.T., Bevilacqua, A., Bursik, M.I., Patra, A.K., 2019. Dynamic probabilistic hazard mapping in the Long Valley Volcanic Region CA: integrating vent opening maps and statistical surrogates of physical models of pyroclastic density currents. J. Geophys. Res. Solid Earth 124 (9), 9600–9621. https://doi.org/10.1029/2019JB01735.
Sandri, L., Thouret, J., Constantinescu, R., 2014. Long-term multi-hazard assessment for El Misti volcano (Peru). Bull. Volcanol. 76 (2). https://doi.org/10.1007/s00445-013-0771-9.
Scollo, S., Tarantola, S., Bonadonna, C., Coltelli, M., Saltelli, A., 2008. Sensitivity analysis and uncertainty estimation for tephra dispersal models. J. Geophys. Res. 113. https://doi.org/10.1029/2006jb004864.
Scott, D.W., 1979. On optimal and data-based histograms. Biometika 66, 605–610.
Sheldrake, T., Caricchi, L., 2017. Regional variability in the frequency and magnitude of large explosive volcanic eruptions. Geology 45 (2), 111–114. https://doi.org/10.1130/G38372.1.
Sheridan, M.F., Stinton, A.J., Patra, A., Pitman, E.B., Bauer, A., Nichita, C.C., 2005. Evaluating Titan2D mass-flow model using the 1963 Little Tahoma Peak avalanches,M ount Rainier, Washington. J. Volcanol. Geotherm. Res. 139, 89–102. https://doi.org/10.1016/j.jvolgeores.2004.06.011.
Situmorang, T., Hadisantono, R.D., 1992. Geological Map of Gede Volcano, Cianjur, West java.
Sparks, R.S.J., Young, S.R., 2002. The eruption of Soufrière Hills Volcano, Montserrat (1995-1999): overview of scientific results. In: Druitt, T.H., Kokelaar, B.P. (Eds.), The eruption of Soufrière Hills Volcano, Montserrat, from 1995 to 1999, 21st ed. Geological Society of London, Memoirs, London, pp. 45–69.
Sparks, R.S.J., Bursik, M.I., Carey, S.N., Gilbert, J.S., Glaze, L.S., Sigurdsson, H., Woods, A.W., 1997. Volcanic Plumes. John Wiley & Sons, Chichester p 574.
Stefanescu, E.R., Bursik, M.I., Patra, A.K., 2012. Effect of digital elevation model on Mohr-Coulomb geophysical flow model output. Nat. Hazards 62 (2), 635–656.
Sulpizio, R., Capra, L., Sarocchi, D., Saucedo, R., Gavilanes-ruiz, J.C., Varley, N.R., 2010. Predicting the block-and-ash flow inundation areas at Volcán de Colima (Colima, Mexico) based on the present day (February 2010) status. J. Volcanol. Geotherm. Res. 193 (1–2), 49–66. https://doi.org/10.1016/j.jvolgeores.2010.03.007.
Suzuki, T., 1983. A theoretical model for the dispersion of tephra. In: Shimozuru, D., Yokoyama, I. (Eds.), Arc Volcanism, Physics and Tectonics. Terra Scientific Publishing, Tokyo, pp. 95–113.
Takahashi, T., Tsujimoto, H., 2000. A mechanical model for Merapi-type pyroclastic flows. J. Volcanol. Geotherm. Res. 98, 91–115. https://doi.org/10.1016/S0377-0273(99)00193-6.
Tierz, P., 2020. Long-term probabilistic volcanic hazard assessment using open and non-open data: observations and current issues. Front. Earth Sci. 8, 1–11. https://doi.org/10.3389/feart.2020.00257.
Tierz, P., Stefanescu, E.R., Sandri, L., Sulpizio, R., Valentine, G.A., Marzocchi, W., Patra, A.K., 2018. Towards quantitative volcanic risk of pyroclastic density currents: probabilistic hazard curves and maps around Somma-Vesuvius (Italy). J. Geophys. Res. Solid Earth 123 (8), 6299–6317. https://doi.org/10.1029/2017JB015383.
Tsuji, T., Ikeda, M., Kishimoto, H., Fujita, K., Nishizaka, N., Onishi, K., 2017. Tephra fallout hazard assessment for VEI5 Plinian Eruption at Kuju Volcano, Japan, using TEPHRA2. IOP Conf. Ser. Earth Environ. Sci. 71 (1). https://doi.org/10.1088/1755-1315/71/1/012002.
Vázquez, R., Macías, J.L., Arce, J.L., Cisneros, G., Saucedo, R., 2019. Numerical simulation of block-and-ash flows for different eruptive scenarios of the Tacaná Volcanic complex, México-Guatemala. J. Volcanol. Geotherm. Res. 373, 36–50. https://doi.org/10.1016/j.jvolgeores.2019.01.026.
Volentik, A., Connor, C., Connor, L., Bonadonna, C., 2009. Aspects of volcanic hazard assessment for the Bataan nuclear power plant, Luzon Peninsula, Philippines. In: Connor, C.,

Chapman, N., Connor, L. (Eds.), Volcanic and Tectonic Hazard Assessment for Nuclear Facilities. Cambridge University Press, Cambridge, pp. 229–256 https://doi.org/10.1017/CBO9780511635380.010.

White, J.T., Connor, C.B., Connor, L., Hasenaka, T., 2017. Efficient inversion and uncertainty quantification of a tephra fallout model. J. Geophys. Res. Solid Earth 122, 281–294. https://doi.org/10.1002/2016JB013682.

Widiwijayanti, C., Hidayat, D., Voight, B., Patra, A., Pitman, E.B., 2007. Modelling dome-collapse pyroclastic flows for crisis assessments on Montserrat with TITAN2D. Cities on Volcanoes 5 Conference, Shimabara, Japan 11-P-34.

Widiwijayanti, C., Voight, B., Hidayat, D., 2008. Objective rapid delineation of areas at risk from block-and-ash pyroclastic flows and surges. Bull. Volcanol. 71, 687–703. https://doi.org/10.1007/s00445-008-0254-6.

Williams, G.T., Jenkins, S.F., Biass, S., Wibowo, H.E., Harijoko, A., 2020. Remotely assessing tephra fall building damage and vulnerability: Kelud Volcano, Indonesia. J. Appl. Volcanol. 9 (1), 1–18. https://doi.org/10.1186/s13617-020-00100-5.

Wilson, L., Sparks, R.S.J., Huang, T.C., Watkins, N.D., 1978. The control of volcanic column heights by eruption energetics and dynamics. J. Geophys. Res. Solid Earth 83, 1829–1836. https://doi.org/10.1029/jb083ib04p01829.

Winson, A.E.G., 2016. Multiparametric Quantification of Volcanic Hazards for Eruption Forecasting and Communication. PhD thesis. Nanyang Technological University, Singapore.